CEIS TOR VERGATA Research Papers

Università di Roma Tor Vergata

ISSN 2610-931X

CEIS Tor Vergata

RESEARCH PAPER SERIES

Vol. 22, Issue 6, No. 589 – December 2024

Multivariate Rough Volatility

Ranieri Dugo, Giacomo Giorgio and Paolo Pigato

Multivariate Rough Volatility

Ranieri Dugo* Giacomo Giorgio† Paolo Pigato‡

December 18, 2024

Abstract

Motivated by empirical evidence from the joint behavior of realized volatility time series, we propose to model the joint dynamics of log-volatilities using a multivariate fractional Ornstein-Uhlenbeck process. This model is a multivariate version of the Rough Fractional Stochastic Volatility model proposed in Gatheral, Jaisson, and Rosenbaum, *Quant. Finance*, 2018. It allows for different Hurst exponents in the different marginal components and non trivial interdependencies.

We discuss the main features of the model and propose an estimator that jointly identifies its parameters. We derive the asymptotic theory of the estimator and perform a simulation study that confirms the asymptotic theory in finite sample.

We carry out an extensive empirical investigation on all realized volatility time series covering the entire span of about two decades in the Oxford-Man realized library. Our analysis shows that these time series are strongly correlated and can exhibit asymmetries in their cross-covariance structure, accurately captured by our model. These asymmetries lead to spillover effects that we analyse theoretically within the model and then using our empirical estimates. Moreover, in accordance with the existing literature, we observe behaviors close to non-stationarity and rough trajectories.

Keywords: stochastic volatility, rough volatility, realized volatility, multivariate time series, volatility spillovers, mean reversion.
JEL Classification: C32, C51, C58, G17.

*Department of Economics and Finance, University of Rome Tor Vergata, ranieri.dugo@students.uniroma2.eu
†Department of Mathematics, University of Rome Tor Vergata, giorgio@mat.uniroma2.it
‡Department of Economics and Finance, University of Rome Tor Vergata, paolo.pigato@uniroma2.it

Acknowledgements: We are grateful to Tommaso Proietti, Stefano De Marco, Davide Pirino, to the participants to the 4th Meeting in Probability in Rome, the QFFE24 in Marseille, and the VI Aarhus Workshop in Econometrics for early feedback. We thank J.-F. Coeurjolly for sharing the code for simulating the multivariate fractional Brownian Motion. Funding: PP was supported by the project PRICE, financed by the Italian Ministry of University and Research under the program PRIN 2022, Prot. 2022C799SX.

1 Introduction

We consider the log-normal, fractional model proposed in Comte and Renault (1998) and Gatheral et al. (2018) for volatility time series and introduce a multivariate extension, where the dynamics of the multivariate log-volatility is specified by an Ornstein-Uhlenbeck process driven by the multivariate fractional Brownian motion (mfBm) in the sense of Amblard et al. (2010), a process that we have analysed in Dugo et al. (2024). The marginal components are one dimensional fractional Ornstein-Uhlenbeck processes, consistently with the established literature on fractional and rough volatility, with Hurst regularity parameter that can be different in each component. The cross-correlation between each two components is ruled by one parameter related to the contemporaneous correlation, and another parameter related to the time reversibility of the process. Both are inherited from the driving mfBm.

We estimate the parameters of the model using a Minimum Distance Estimation procedure (Tieslau et al. 1996), which aims at matching model-implied and empirical cross-covariances. First, we derive the asymptotic theory of the estimator, proving speed of convergence and asymptotic normality, and perform an extensive simulation study that confirms these results in finite sample. Then, we estimate the model on 20 years of 22 realized volatility time series data from the Oxford-Man library, finding a remarkably good fit, particularly with respect to cross-correlations and their possibly asymmetric decay as a function of the time lag, which seems to be related to the Hurst exponents of the components as predicted by our model. These asymmetries suggest the presence of spillover effects between components, which we analyse theoretically within the model, in the framework of Diebold and Yilmaz (2012), and then empirically using the parameter estimates obtained in sample. Our analysis also suggests, consistently with the known literature, roughness in the trajectories and behaviors close to non-stationarity.

Background: A mean-reverting, fractional, Gaussian volatility model, able to reproduce the long-memory behavior of realized volatility, and based on the fractional Ornstein-Uhlenbeck process (see Cheridito et al. 2003), was first introduced in Comte and Renault (1998). Estimations of this model on empirical data, on short time lags, have subsequently hinted to extremely small Hurst parameters for realized volatility trajectories, supporting the "rough volatility" specification by Gatheral et al. (2018). The empirical rough behavior of the trajectories of this model has been confirmed by a number of econometrical studies (Bolko et al. 2023; Wang et al. 2023; Eumenius-Schulz 2020; Bianchi et al. 2023), and the estimation of similar models also points to rough behavior of the realized volatility trajectories (Bennedsen et al. 2021; Chong et al. 2024b; Chong et al. 2024a; Fukasawa et al. 2022; Livieri et al. 2018). The fact that empirical log-volatility is mean-reverting, Gaussian, and exhibits fractional features is well established (Fouque et al. 2000; Andersen et al. 2001; Ding and Granger 1996). The rough volatility specification, moreover, is supported by the option pricing literature with particular attention to the implied volatility skew (Bayer et al. 2016; Bayer et al. 2019; Friz et al. 2022; Livieri et al. 2018; Delemotte et al. 2023, see also Guyon and El Amrani 2023).

Concerning the modelling of multivariate time series and their cross memory structure, let us mention Podobnik et al. (2010), Podobnik et al. (2007), Wang et al. (2011), and Podobnik et al. (2008), where applications to economics, but also to physics, physiology, and genomics, are considered. Time-reversibility has also been widely considered in the financial literature, at least in the unidimensional setting (see e.g. Zumbach 2009; Cordi et al. 2021).

Outline: Section 2 introduces and describes the model. Section 3 develops the estimation procedure and its asymptotic properties. Section 4 evaluates the estimator finite-sample performance through simulations. Section 5 details the empirical estimation results. Section 6 examines spillover effects. Section 7 concludes. Proofs and supplementary results are provided in the Appendix, with additional empirical analyses and reproducible code available online.

2 The Model

The model we propose for the logarithm of realized volatility is a multivariate version of the Rough Fractional Stochastic Volatility model by Gatheral et al. (2018). It is the solution to a mean-reverting stochastic differential equation (SDE) driven by the mfBm by Amblard et al. (2010). We introduced this continuous-time process, that we call multivariate fractional Ornstein-Uhlenbeck (mfOU) process, in Dugo et al. (2024).

Let $(W_t^H)_t = (W_t^{H_1}, \dots, W_t^{H_N})_t$, be a mfBm, i.e. a vector-valued Gaussian process in dimension N

with parameters $H \in (0,1)^N$, $\rho \in [-1,1]^{N\times N}$, and $\eta \in \mathbb{R}^{N\times N}$. In this context, $H = (H_1, \dots, H_N)$ is the vector of Hurst exponents of the components, the matrix ρ represents the contemporaneous correlation of the mfBm at each point in time, and the matrix η is related to the asymmetry in time of the cross-covariance function and the time reversibility of the process. These matrices are such that $\rho_{i,i} = 1$, $\rho_{i,j} = \rho_{j,i}$, $\eta_{i,i} = 0$, and $\eta_{i,j} = -\eta_{j,i}$ for $i, j = 1, \dots, N$. In addition, the parameters H_i, $\rho_{i,j}$, and $\eta_{i,j}$ need to satisfy pairwise coherency constraints, $c(H_i, H_j, \rho_{i,j}, \eta_{i,j}) \leq 1$, $\forall i, j = 1, \dots, N$, in order to have a well-defined covariance function (see Dugo et al. 2024).

The mfOU process, $(Y_t)_t = (Y_t^1, \dots, Y_t^N)_t$, is the vector process whose components solve pathwise (Cheridito et al. 2003) equations

$$dY_t^i = \alpha_i(\mu_i - Y_t^i)dt + \nu_i dW_t^{H_i}, \qquad i = 1, \dots, N, \tag{1}$$

where $\mu_i \in \mathbb{R}$ is the long-term mean, $\nu_i > 0$ is the diffusion coefficient, and $\alpha_i > 0$ is the speed of mean reversion. Let us write $\nu = (\nu_1, \dots, \nu_N)$ and $\alpha = (\alpha_1, \dots, \alpha_N)$. Equation (1) has a stationary solution given by

$$Y_t^i = \mu_i + \nu_i \int_{-\infty}^{t} e^{-\alpha_i(t-s)} dW_s^{H_i}, \qquad i = 1, \dots, N. \tag{2}$$

This is an autoregressive process, as one can see writing

$$Y_t^i = e^{-\alpha_i \Delta} Y_{t-\Delta}^i + \left(1 - e^{-\alpha_i \Delta}\right) \mu_i + \nu_i \int_{t-\Delta}^{t} e^{-\alpha_i(t-s)} dW_s^{H_i}, \qquad i = 1, \dots, N.$$

In this work, we assume to observe the log-volatility process at the stationary regime. Its expectation is

$$\mathbb{E}\left[Y_t\right] = \mu = (\mu_1, \dots, \mu_N).$$

Let us denote $\gamma_{i,j}(k) := \mathrm{Cov}(Y_{t+k}^i, Y_t^j)$, $k \in \mathbb{R}$, the cross-covariance function. We assume here $H_{i,j} = H_i + H_j \neq 1$, in which case

$$\gamma_{i,j}(k) = e^{-\alpha_j k}\gamma_{i,j}(0) + \nu_i \nu_j e^{-\alpha_j k} H_{i,j}(H_{i,j} - 1)\frac{\rho_{i,j} + \eta_{i,j}}{2} \int_0^k e^{\alpha_j v} \left(\int_{-\infty}^{0} e^{\alpha_i u}(v-u)^{H_{i,j}-2} du \right) dv, \tag{3}$$

where the covariance, $\gamma_{i,j}(0)$, is

$$\gamma_{i,j}(0) = \frac{\Gamma(H_{i,j}+1)\nu_i\nu_j}{2(\alpha_i + \alpha_j)} \left(\left(\alpha_i^{1-H_{i,j}} + \alpha_j^{1-H_{i,j}} \right) \rho_{i,j} + \left(\alpha_j^{1-H_{i,j}} - \alpha_i^{1-H_{i,j}} \right) \eta_{i,j} \right).$$

In Dugo et al. (2024) we showed that the cross-covariance decays as a power law with exponent $H_{i,j} - 2$, as $k \to \infty$, therefore allowing for long-range interdependence (meaning that the cross-covariance is not integrable) when $H_{i,j} > 1$, in analogy to long-memory in the univariate case. Note that a different expression holds for the covariance function when $H_{i,j} = 1$, which corresponds to a discontinuity of the cross-covariance as a function of the Hurst exponents.

In line with the univariate case treated by Gatheral et al. (2018), if the mean reversion coefficients are small, the process behaves locally as a mfBm.

Proposition 1. *Let $\left(W_t^H\right)_t$ be a mfBm, $(Y_t)_t$ be the mfOU process in (2). Then, as $\alpha \to 0$,*

$$\mathbb{E}\left[\sup_{t\in[0,T]} \left|\left| Y_t - Y_0 - \nu \odot W_t^H \right|\right| \right] \to 0,$$

where $||\cdot||$ represent the L^2 norm and $\odot$ indicates the Hadamard product.

Proof. Follows from the univariate result in Gatheral et al. (2018).

Note that $\gamma_{i,j}(k)$ and $\gamma_{i,j}(0)$ depend on α_i and α_j. In the regime of slow mean reversion, the cross-covariance function of mfOU is approximately linear in $k^{H_{i,j}}$.

Proposition 2. *For $H_{i,j} < 1$ and fixed $k > 0$, as $(\alpha_i, \alpha_j) \to (0,0)$,*

$$\gamma_{i,j}(k) = \gamma_{i,j}(0) - \frac{\rho_{i,j} + \eta_{i,j}}{2} \nu_i \nu_j k^{H_{i,j}} + o(1).$$

Proof. Follows by taking the limit in (3) and standard computations.
An analogous approximation result holds taking $k \to 0$ instead of $(\alpha_i, \alpha_j) \to (0,0)$ (see Dugo et al. 2024).

3 Estimation method

In order to jointly estimate all the parameters in our model, we consider a suitable loss function. The parameters count to $p = N(N+2)$, including $N \times 3$ parameters governing the marginal distributions, specifically α_i, ν_i, and H_i for $i = 1, \ldots, N$, and $N(N-1)/2$ parameters in each of the matrices ρ and η, determining the multivariate dynamics. We subtract the sample mean from the observations of the process in the beginning, so we do not deal with μ_i.

We define the parameter vector $\theta = (\alpha_i, \nu_i, H_i, \rho_{i,j}, \eta_{i,j},\ i = 1, \ldots, N,\ i < j < N) \in \Theta \subset \mathbb{R}_+^N \times \mathbb{R}_+^N \times (0,1)^N \times [-1,1]^{N(N-1)/2} \times \mathbb{R}^{N(N-1)/2}$, which represents the full set of parameters to be estimated. While maximizing the likelihood function would be the most efficient approach, the non-Markovian nature of the process makes this computationally infeasible. In Amblard and Coeurjolly (2011), discrete filtering techniques are used in this context to estimate the mfBm. Here, we adopt a Minimum Distance Estimator (MDE) in the spirit of Tieslau et al. (1996), which can be seen as a specific case of the Generalized Method of Moments (Hansen 1982).

In the MDE approach, we consider an overdetermined system of equations in the parameters to be estimated, which we call moment conditions. The estimator is defined as the parameter value that is closest, in a mean-square sense, to solving the system. Let $(Y_{i\Delta})_{i=0}^n$ be a set of $n \in \mathbb{N}$ discrete observations of the process over the interval $[0,T]$, observed at time intervals $\Delta = T/n$. Our goal is for the model-implied cross-covariances, calculated with the estimated parameters $\gamma_{i,j}^k(\hat{\theta})$, to be as close as possible to sample cross-covariances

$$\hat{\gamma}_{i,j}^k = \frac{1}{n-k} \sum_{l=1}^{n-k} \left(Y_{l+k}^i - \hat{\mu}_i\right) \left(Y_l^j - \hat{\mu}_j\right),$$

where $\hat{\mu}_i = \frac{1}{n} \sum_{l=1}^n Y_l^i,\ i = 1, \ldots, N$ are computed in our framework before the optimization takes place.

We define the vectors that contain, respectively, model and sample cross-covariances, ordered consistently, in the obvious manner:

$$\gamma(\theta) = \left(\left(\gamma_{ij}^k(\theta)\right)_{k \in \mathcal{L},\ i,j=1,\ldots,N}\right)^T \in \mathbb{R}^{N(L+(N-1)(L-1/2))},$$
$$\hat{\gamma}_n = \left(\left(\hat{\gamma}_{ij}^k\right)_{k \in \mathcal{L},\ i,j=1,\ldots,N}\right)^T \in \mathbb{R}^{N(L+(N-1)(L-1/2))},$$

where L is the cardinality of the set $\mathcal{L} \subset \mathbb{N} \cup \{0\}$, appropriately chosen (cf. Andersen and Sørensen 1996). We define the MDE estimator $\hat{\theta}$ as the value of θ that minimizes the loss function

$$\mathcal{T}(\theta) = \left(\hat{\gamma}_n - \gamma(\theta)\right)^T W \left(\hat{\gamma}_n - \gamma(\theta)\right),$$

i.e.

$$\hat{\theta}_n = \arg\min_{\theta} \mathcal{T}(\theta), \tag{4}$$

where W is a symmetric, positive definite matrix of order $N(L+(N-1)(L-1/2))$. Stationarity and ergodicity of the mfOU process, together with the regularity of the cross-covariance function, imply the following.

Proposition 3. *Let $\theta_0 \in \Theta$ be the true value of the parameter in the population distributed as the mfOU process. If $H_{i,j} \neq 1,\ \forall i,j = 1, \ldots, N$:*

I. the MDE estimator is consistent, i.e.

$$\hat{\theta}_n \xrightarrow{p} \theta_0 \qquad \text{as } n \to \infty,$$

II. when $\max(H_i,\ i=1,\dots,N) < \frac{3}{4}$*, the MDE estimator is asymptotically normal, i.e.*

$$\sqrt{n}\left(\hat{\theta}_n - \theta_0\right) \xrightarrow{d} N(0,\Sigma) \qquad \text{as } n \to \infty,$$

where $\Sigma = \left(J_\gamma^T W J_\gamma\right)^{-1} J_\gamma^T W \Gamma W J_\gamma \left(J_\gamma^T W J_\gamma\right)^{-1}$*,* $J_\gamma := J_\gamma(\theta_0) = \partial\gamma(\theta)/\partial\theta|_{\theta_0}$ *is the Jacobian matrix of* $\gamma(\theta)$ *at* θ_0*, and* Γ *is the asymptotic covariance matrix of* $\hat{\gamma}_n$*.*

The proof of the above results is postponed to Appendix A. We expect, but do not prove here, a non-Gaussian result to hold if $\max(H_i,\ i=1,\dots,N) > 3/4$, similarly to Dugo et al. 2024.

Remark 1. *The inequality*

$$(J_\gamma^T W J_\gamma)^{-1} J_\gamma^T W \Gamma W D (J_\gamma^T W J_\gamma)^{-1} - (J_\gamma^T \Gamma^{-1} J_\gamma)^{-1} \geq 0,$$

suggests that higher efficiency for $\hat{\theta}$ *could be achieved by choosing* $W = \Gamma^{-1}$*, which delivers the lowest asymptotic variance* $\Sigma^* = (J_\gamma^T \Gamma^{-1} J_\gamma)^{-1}$*. This is the the optimal weighting used in generalized linear models (see Hayashi 2011 for details). However, at present* Γ *appears intractable for the mfOU process (see Appendix A), so we proceed with the identity matrix* $W := I$*. We leave developing a computable expression for* Γ *and/or exploring its estimation as a possible future improvement of the method.*

We solve the optimization in (4) numerically, using initial conditions provided by a 2-step estimator that combines the univariate estimators from Wang et al. (2023) with those from Dugo et al. (2024) for the correlation parameters. We perform the numerical optimization with the L-BFGS-B algorithm within the *optim()* function in R 4.3.3.

4 Monte Carlo study

In this section, we evaluate the accuracy of the MDE procedure on synthetic data.

4.1 Simulation method

We simulate the mfOU process via the Euler-Maruyama scheme in combination with a circulant embedding scheme for the driving fractional Gaussian noise, which is an exact simulation method for stationary Gaussian processes initially introduced by Wood and Chan (1994) and later adapted by Amblard et al. (2010) to the mfBm.

We want a discrete trajectory on the uniform partition with mesh Δ of the interval $[0,T]$. Given a set of parameters $(\alpha_i, H_i, \nu_i, \mu_i,\ i=1,\dots,N)$, we produce M time series of length $n = T/\Delta$ repeating the following procedure.

1) We start with a longer horizon $T^\star > T$ and a finer partition $\delta < \Delta$. The preliminary period $T^\star - T$ is necessary to obtain realizations from the stationary distribution while the finer partition $\delta < \Delta$ is used to reduce the discretization error induced by the Euler-Maruyama scheme.

2) We produce a sequence of $n^\star = T^\star/\delta$ multivariate fractional Gaussian noises (mfGn) of Hurst exponents $H_1,\dots,H_N$ given by the increments of the mfBm over the intervals of size δ,

$$\left(W_{j\delta}^{H_1} - W_{(j-1)\delta}^{H_1}, \dots, W_{j\delta}^{H_N} - W_{(j-1)\delta}^{H_N}\right)_{j=1}^{n^\star},$$

with the circulant embedding scheme proposed in Amblard et al. 2010.

3) Starting from $Y_0^i,\ i=1,\dots,N$ drawn from the stationary distribution, and the mfGn obtained at the previous step, we calculate the Euler-Maruyama scheme for the mfOU process on the finer grid with mesh δ,

$$Y_{j\delta}^i = Y_{(j-1)\delta}^i + \alpha_i\left(\mu_i - Y_{(j-1)\delta}^i\right)\delta + \nu_i\left(W_{j\delta}^{H_i} - W_{(j-1)\delta}^{H_i}\right),$$

for $j = 1,\dots,n^\star$, $i = 1,\dots,N$.

4) We discard the first $(T^\star - T)/\delta$ observations so as to obtain T/δ observations of the process at the stationary regime and retain a subset $(Y_{j\Delta})_{j=0}^{n}$ of observations at intervals Δ, for which the discretization error is smaller, from the finer discretized trajectory $(Y_{j\delta})_{j=0}^{T/\delta}$.

For each set of parameters considered in the following, the previous methodology is implemented with $N = 2,\ \mu_i = 0,\ i = 1, 2,\ \delta = 1/(252 \times 2^{10}),\ \Delta = 1/252,\ T^\star = 28,\ T = 20$, and $M = 10^4$. The values for Δ and T are similar to the daily observations over roughly 20 years in the dataset employed in the empirical analysis.

4.2 Finite sample performance

We conduct Monte Carlo (MC) simulations across seven different parameter sets to examine how the estimator behaves with varying values of $\alpha_i, H_i,$ and $\eta_{i,j}$. We focus on a bivariate model where α_i and H_i vary jointly for $i = 1, 2$. Following Bolko et al. (2023), we use the set of lags $\mathcal{L} = (0,\ 1,\ 2,\ 3,\ 4,\ 5,\ 20,\ 50)$, which yields 31 moment conditions with 23 overidentifying restrictions. See Andersen and Sørensen (1996) for a discussion on the choice of $\mathcal{L}$.

Table 1 presents the results. Each panel, labeled A through G, reports the true parameter values (True), the average of point estimates across MC samples (Avg), the MC sample standard deviation (Std Err), and the bias (Bias = Avg - True).

Panel A represents the baseline scenario, reflecting estimates obtained from the logarithm of realized volatility time series for the pair FCHI - FTSE in the empirical analysis of Section 5. Here, we find reliable estimates for all parameters except for α_1 and α_2, which display slight upward biases - consistently with prior findings in the literature (Wang et al. 2023). Standard errors remain low and the biases are null for the remaining parameters. When $\alpha_i,\ i = 1, 2$ decrease (Panel B and C), their upward biases grow. These biases, which do not affect other parameters' biases or standard errors, reflect biases in the covariances, which appear when $\alpha_i,\ i = 1, 2$ shrink. These are transferred to the estimates of $\alpha_i,\ i = 1, 2$ but not to the other parameters. The MDE estimator shows lower biases in $\alpha_i,\ i = 1, 2$ than the 2-step one used for the initial conditions.

Let us now focus on varying values of $H_i,\ i = 1, 2$ in Panel D and E. When $H_i = 0.45,\ i = 1, 2$, we observe slightly higher standard errors and biases in the parameter estimates, due to the vicinity to the region $H_{i,j} = 1$, where the cross-covariance function, $\gamma_{i,j}^{k}(\theta)$, is discontinuous. For $H_i = 0.7,\ i = 1, 2$, standard errors and biases also increase for some parameters but less than in the previous case, now due to the fact that we are getting closer to the region $H_i > 3/4$, where the sample average estimator of the cross-covariance does not admit a Gaussian central limit theorem.

Finally, in Panels F and G, we increase $\eta_{1,2}$ to 0.1 and 0.2, respectively, without observing notable deviations from the baseline behavior. More extreme values for $\eta_{1,2}$ are not allowed by the coherency constraint (cf. Section 2).

In general, the MDE estimator shows lower standard errors compared to the initial 2-step estimator, especially for $\alpha_i,\ i = 1, 2,\ \rho_{1,2}$, and $\eta_{1,2}$.

Table 1: Finite sample performance of the MDE estimator, $\hat{\theta}$, on simulated mfOU processes. Baseline scenario (True) corresponding to empirical estimates for the pair FCHI - FTSE from Section 5. Point estimates (Avg), standard errors (Std Err), and biases (Bias) are computed as MC averages. Simulation parameters: $N = 2,\ M = 10^4,\ \Delta = 1/252,\ T = 20,\ \mu_i = 0,\ i = 1, 2$.

	α_1	α_2	ν_1	ν_2	H_1	H_2	$\rho_{1,2}$	$\eta_{1,2}$
				Panel A				
True	**1.32**	**1.45**	**0.78**	**0.79**	**0.19**	**0.21**	**0.94**	**0.00**
Avg	1.48	1.61	0.79	0.79	0.20	0.21	0.94	0.00
Std Err	0.56	0.58	0.05	0.05	0.02	0.02	0.01	0.02
Bias	0.16	0.16	0.00	0.01	0.00	0.00	0.00	0.00
				Panel B				
True	**0.50**	**0.50**	0.78	0.79	0.19	0.21	0.94	0.00

Continued on next page

	α_1	α_2	ν_1	ν_2	H_1	H_2	$\rho_{1,2}$	$\eta_{1,2}$
Avg	0.68	0.68	0.79	0.80	0.20	0.21	0.94	0.00
Std Err	0.38	0.38	0.05	0.05	0.02	0.02	0.01	0.01
Bias	0.18	0.18	0.00	0.00	0.00	0.00	0.00	0.00
				Panel C				
True	**0.05**	**0.05**	0.78	0.79	0.19	0.21	0.94	0.00
Avg	0.29	0.29	0.79	0.80	0.20	0.21	0.95	0.00
Std Err	0.28	0.27	0.06	0.06	0.02	0.02	0.04	0.03
Bias	0.24	0.24	0.00	0.00	0.00	0.00	0.00	0.00
				Panel D				
True	1.32	1.45	0.78	0.79	**0.45**	**0.45**	0.94	0.00
Avg	1.70	1.85	0.83	0.85	0.47	0.47	0.94	-0.01
Std Err	0.72	0.76	0.14	0.14	0.05	0.05	0.02	0.43
Bias	0.39	0.41	0.05	0.05	0.02	0.02	0.00	-0.01
				Panel E				
True	1.32	1.45	0.78	0.79	**0.70**	**0.70**	0.94	0.00
Avg	1.73	1.73	0.79	0.80	0.69	0.69	0.94	0.01
Std Err	0.55	0.57	0.09	0.09	0.05	0.05	0.03	0.11
Bias	0.41	0.42	0.01	0.01	-0.01	-0.01	0.00	0.01
				Panel F				
True	1.32	1.45	0.78	0.79	0.19	0.21	0.94	**0.10**
Avg	1.49	1.61	0.79	0.80	0.20	0.21	0.94	0.10
Std Err	0.18	0.16	0.01	0.01	0.00	0.00	0.00	0.00
Bias	0.18	0.16	0.01	0.01	0.00	0.00	0.00	0.00
				Panel G				
True	1.32	1.45	0.78	0.79	0.19	0.21	0.94	**0.20**
Avg	1.49	1.62	0.79	0.80	0.20	0.21	0.94	0.20
Std Err	0.58	0.59	0.06	0.05	0.02	0.02	0.01	0.05
Bias	0.18	0.17	0.01	0.01	0.00	0.00	0.00	0.00

Another perspective on the results of the MC analysis is presented in Figure 1, which shows the estimation error densities. The figure focuses on one parameter at a time, comparing the Nadaraya-Watson density of the standardized estimation errors for each experimental setting (dashed lines) with the standard Gaussian distribution (shaded area). The colors of the dashed lines correspond to the different panels in Table 1.

From the results, we can conclude that a trajectory length of $n = 20 \times 252 = 5040$ is generally sufficient to approximate the normal distribution predicted by the asymptotic theory (Proposition 3). However, notable exceptions are observed in the distributions of the errors for $\alpha_i,\ i = 1, 2$, which exhibit skewness, especially for lower parameter values. Under the same circumstances, a slight skewness is also present in the error distribution for $\rho_{1,2}$. Under the specifications in Panels D and G, where the baseline is modified to $H_i = 0.45,\ i = 1, 2$ and $\eta_{1,2} = 0.2$, respectively, the error distribution for $\eta_{1,2}$ appears excessively peaked. This is due to the discontinuity of $\gamma^k_{i,j}(\theta)$ at $H_i + H_j = 1$ in the first case, and to the fact that the coherency constraint is satisfied by a very small margin in the second case.

4.3 Slow mean reversion

Motivated by the asymptotic expression of the cross-covariance function for $\alpha \to 0$ given in Proposition 2, and the lower-quality results obtained for small $\alpha_i,\ i = 1, 2$ in simulation in Section 4.2, we also attempt minimum distance estimation using the small-alpha cross-covariance approximation in the moment conditions. We include lag-0 variances and covariances ($\mathrm{V}_1,\ \mathrm{V}_2,\ \mathrm{C}_{1,2}$), which appear in the asymptotic formula, as parameters to be estimated in the optimization process. The results are presented in Table 2 and Figure 2.

The results for $\nu_i,\ H_i,\ i = 1, 2,\ \rho_{1,2},$ and $\eta_{1,2}$ are satisfactory. We only observe slight biases in most parameters (Panel A), which vanish as $\alpha_i,\ i = 1, 2$ decrease (Panels B and C). The standard errors are very similar to those obtained using the exact cross-covariance function (3) in Table 1.

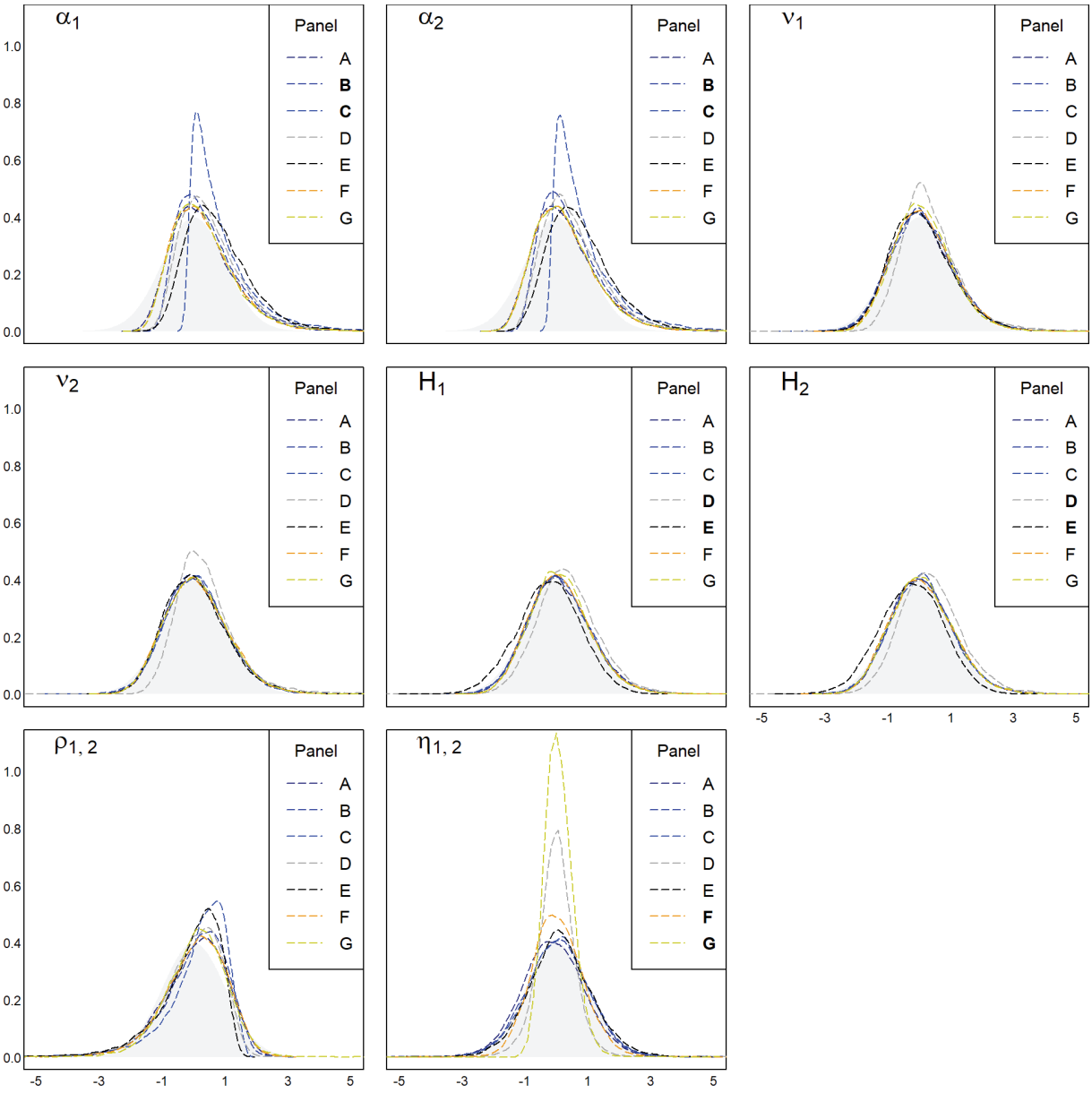

Figure 1: Kernel estimates of the densities of the elements in $(\hat{\theta} - \theta_0)/\widehat{s.e.}(\hat{\theta})$, where $\widehat{s.e.}(\hat{\theta})$ is the MC standard error of the MDE estimator $\hat{\theta}$. Parameter settings are in Table 1. Simulation parameters: $N = 2,\ M = 10^4,\ \Delta = 1/252,\ T = 20,\ \mu_i = 0,\ i = 1, 2$. The bold letters emphasize the parameter being varied within each panel.

However, the same cannot be said for $\mathrm{V}_1,\ \mathrm{V}_2,\ \mathrm{C}_{1,2}$, which exhibit a bias that originates similarly to the one previously associated with $\alpha_i,\ i = 1, 2$. Motivated by this finding, we estimate the cross-covariance using a sample average estimator and observe similar evidence of biases across several lags when $\alpha_i,\ i = 1, 2$ are small. This finding may explain the nature of the bias in the estimator of the mean reversion coefficient in Wang et al. (2023), which relies on the sample variance.

Table 2: Finite sample performance of the MDE estimator based on asymptotic cross-covariance conditions on simulated mfOU process. Baseline scenario (True) corresponding to empirical estimates for the pair FCHI - FTSE from Section 5. Point estimates (Avg), standard errors (Std Err), and biases (Bias) are computed as MC averages. Simulation parameters: $N = 2,\ M = 10^4,\ \Delta = 1/252,\ T = 20,\ \mu_i = 0,\ i = 1, 2$.

	ν_1	ν_2	H_1	H_2	$\rho_{1,2}$	$\eta_{1,2}$	V_1	V_2	$C_{1,2}$
					Panel A				
True	**0.78**	**0.79**	**0.19**	**0.21**	**0.94**	**0.00**	**0.24**	**0.24**	**0.23**
Avg	0.76	0.77	0.19	0.20	0.94	-0.01	0.24	0.24	0.23
Std Err	0.05	0.04	0.01	0.01	0.01	0.02	0.03	0.03	0.03
Bias	-0.02	-0.02	-0.01	-0.01	0.00	-0.01	0.00	0.00	0.00
					Panel B				
True	0.78	0.79	0.19	0.21	0.94	0.00	**0.35**	**0.37**	**0.34**
Avg	0.78	0.79	0.19	0.21	0.94	0.00	0.34	0.36	0.33
Std Err	0.04	0.05	0.01	0.02	0.01	0.02	0.07	0.08	0.07
Bias	0.00	0.00	0.00	0.00	0.00	0.00	-0.01	-0.02	-0.01
					Panel C				
True	0.78	0.79	0.19	0.21	0.94	0.00	**0.87**	**0.97**	**0.87**
Avg	0.78	0.80	0.19	0.21	0.94	0.00	0.57	0.61	0.56
Std Err	0.05	0.06	0.02	0.02	0.01	0.03	0.24	0.27	0.25
Bias	0.00	0.00	0.00	0.00	0.00	0.00	-0.30	-0.36	-0.31

Similar conclusions can be drawn from the estimation error densities shown in Figure 2. They are slightly skewed in the baseline scenario (darkest line) but quickly become centered and resemble a Gaussian distribution as the mean reversion coefficients decrease. In contrast, the variances $(\mathrm{V}_1,\ \mathrm{V}_2)$ and the covariance $(\mathrm{C}_{1,2})$ grow increasingly skewed and non-normal.

5 Empirical analysis

Our empirical study utilizes realized volatility time series based on 5-minute price increments from the Realized Library of the Oxford-Man Institute.[1] The dataset we use spans over 20 years of daily observations, starting from January 3, 2000, to June 28, 2022. It includes realized volatilities for 31 indices associated with stock exchanges worldwide. We retain only the series covering the entire sample period and discard the ones that have sequences of missing values at the beginning, middle, or end of the sample. The final sample is composed of 22 time series, each averaging 5616 observations. We treat this collection as a multivariate system after removing observations with a realized volatility equal to zero, scaling to annual percentage points, and applying the logarithm transformation. A detailed description of the dataset can be found in Appendix B.

5.1 Estimates

Table 3, 4, and 5 present the estimates obtained with the procedure described in Section 3 on the Oxford-Man dataset. We employ the MDE estimation procedure with the same lags as for the MC study, i.e. $\mathcal{L} = (0,\ 1,\ 2,\ 3,\ 4,\ 5,\ 20,\ 50)$, and $\Delta = 1/252$. Since $L = \#\mathcal{L} = 8$ and $N = 22$, we now have 528 parameters and 3641 moment conditions.

[1] https://oxford-man.ox.ac.uk/research/realized-library (no longer accessible)

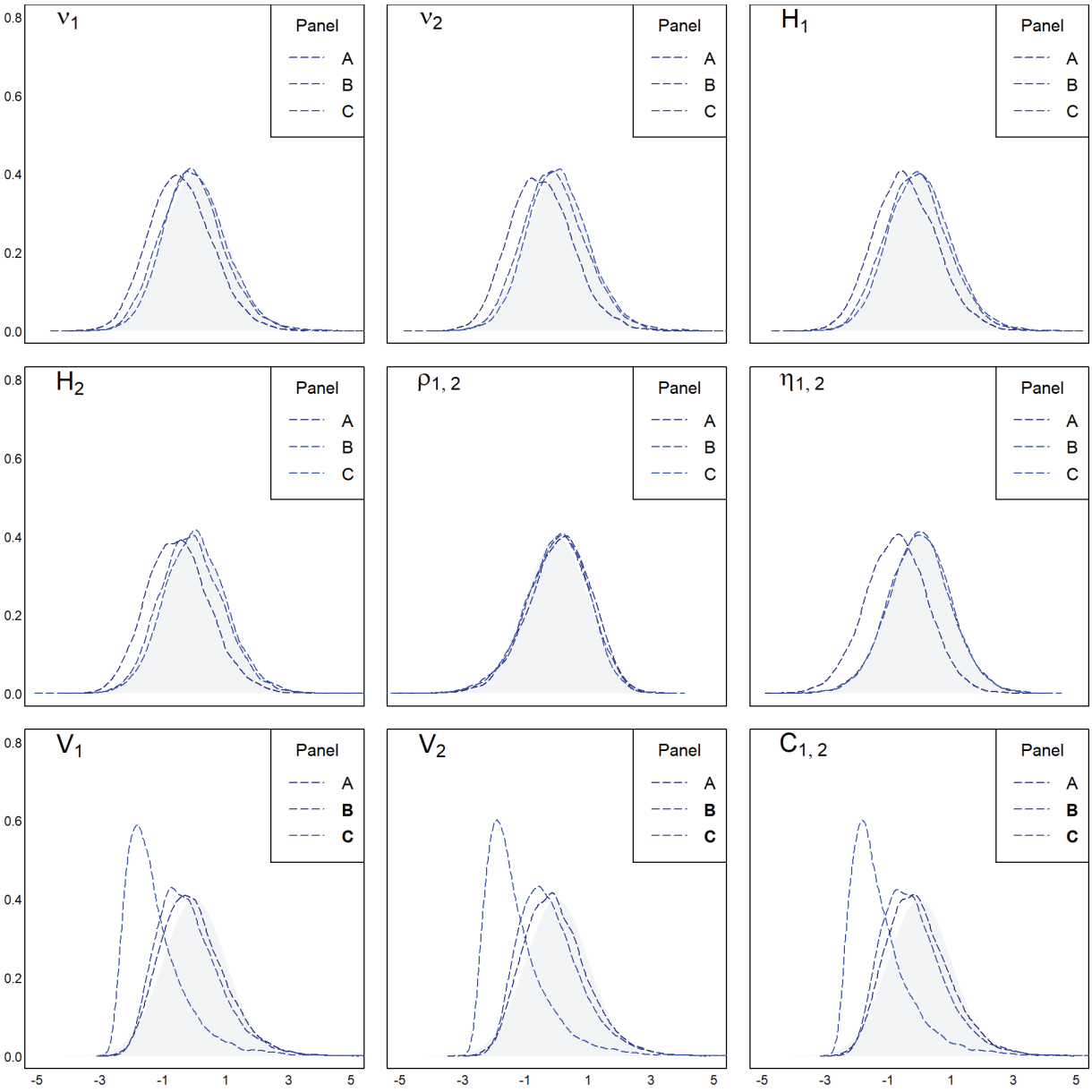

Figure 2: kernel estimates of the densities of the elements in $(\hat{\theta}-\theta_0)/\widehat{s.e.}(\hat{\theta})$, where $\hat{\theta}$ denotes the MDE estimator that uses asymptotic cross-covariance conditions, and $\widehat{s.e.}(\hat{\theta})$ is the MC standard error of $\hat{\theta}$. Parameter settings are in Table 2. Simulation parameters: $N = 2,\ M = 10^4,\ \Delta = 1/252,\ T = 20,\ \mu_i = 0,\ i = 1, 2$. The bold letters emphasize the parameter being varied within each panel.

Table 3: Estimates of the univariate marginal parameters on $\log\left(100\sqrt{RV \times 252}\right)$, where RV is the realized variance from Oxford-Man (rv5). The MDE estimates are shown above and the initial values from the 2-step procedure are shown below among parentheses. The MDE procedure uses $\mathcal{L} = \{0,\ 1,\ 2,\ 3,\ 4,\ 5,\ 20,\ 50\}$ and $\Delta = 1/252$. The 2-step procedure corresponds to the estimator in Wang et al. (2023). Symbol is based on the provider convention.

Symbol	μ	α	H	ν	**Symbol**	μ	α	H	ν
S5E	2.679	1.355	0.157	0.833	KSE	2.468	4.263	0.258	1.045
		(0.698)	(0.119)	(0.748)			(6.190)	(0.189)	(1.093)
SSMI	2.395	1.837	0.244	0.785	KS11	2.540	2.004	0.393	0.913
		(0.625)	(0.162)	(0.621)			(0.015)	(0.104)	(0.486)
IBEX	2.698	1.736	0.207	0.808	HSI	2.536	1.852	0.259	0.694
		(1.294)	(0.171)	(0.737)			(0.000)	(0.041)	(0.371)
GDAXI	2.680	1.471	0.213	0.856	BSESN	2.640	1.409	0.188	0.763
		(0.230)	(0.130)	(0.640)			(2.504)	(0.188)	(0.872)
FTSE	2.538	1.446	0.208	0.795	AORD	2.143	2.523	0.283	0.861
		(0.053)	(0.086)	(0.574)			(0.000)	(0.026)	(0.446)
FCHI	2.627	1.316	0.194	0.781	SPX	2.425	1.224	0.185	0.898
		(0.478)	(0.143)	(0.664)			(0.199)	(0.127)	(0.694)
BFX	2.463	1.739	0.223	0.778	RUT	2.351	1.559	0.152	0.833
		(0.417)	(0.138)	(0.615)			(0.886)	(0.127)	(0.738)
AEX	2.529	1.332	0.194	0.806	MXX	2.403	2.413	0.164	0.758
		(0.602)	(0.151)	(0.702)			(0.006)	(0.052)	(0.504)
SSEC	2.669	2.280	0.357	0.989	IXIC	2.537	1.162	0.171	0.860
		(2.469)	(0.196)	(0.941)			(2.025)	(0.206)	(0.953)
NSEI	2.532	0.136	0.118	0.595	DJI	2.442	1.293	0.183	0.867
		(0.942)	(0.144)	(0.768)			(0.014)	(0.083)	(0.573)
N225	2.517	1.768	0.206	0.767	BVSP	2.756	2.654	0.164	0.729
		(1.028)	(0.145)	(0.698)			(6.245)	(0.188)	(0.877)

Table 3 presents the parameters related to the univariate marginal components: the MDE estimates as main figures and the 2-step estimates, which are the starting values in the numerical optimization, provided in parentheses below. The average volatility ranges from 2.143 for AORD to 2.756 for BVSP, with all of them being around 2.5. The mean reversion parameters, α_i, are mostly estimated around 1.6, with some exceptions, most notably NSEI (0.136) and KSE (4.263). The effect of the MDE estimator over the starting values is mainly to increase the estimates, although it sometimes also mitigates very large initial values. The estimates for the Hurst exponent H_i, which rules the regularity of the trajectories and the memory of the process, consistently fall below 1/2. This suggests that the trajectories are rough, with the process exhibiting absence of long memory at the univariate level and short-range interdependence at the multivariate level (cf. Section 2). The MDE routine mostly reduces roughness by increasing the initial values for H_i, obtained with the method in Wang et al. (2023) and Lang and Roueff (2001). Additionally, the values for ν_i mostly increase slightly due to the MDE routine, and a positive empirical correlation of 0.5 is observed between the estimates for H_i and ν_i. Table 4 and 5 present the estimates of the matrices ρ and η. Starting values given by the 2-step procedure are provided below among parenthesis. Table 4 exhibits the results for ρ, the correlation coefficient of the underlying mfBm ($\rho_{i,j} = \rho_{j,i}$). The primary finding is that most values in ρ are high and positive, with fewer than half of the pairs showing values below 0.5. The strongest correlations are observed between the log-volatilities of S5E and FCHI (0.996), as well as SPX and DJI (0.990). Several pairs within Europe or North America display $\rho_{i,j} > 0.9$, indicating that their volatilities tend to fluctuate together closely. In contrast, volatilities in Asia and Oceania (columns between SSEC and AORD) exhibit more

moderate $\rho_{i,j}$ values, with only one pair, NSEI and BSESN, exceeding 0.8 (0.893). The lowest correlations are observed between the volatilities for KSE and several others, or less notably between SSEC and others. Similar conclusions emerge from the graphical representation of the estimates of ρ in Figure 3. The figure displays an undirected graph, where nodes correspond to indices, and edges are inversely proportional to the estimates of $\rho_{i,j}$. This visualization shows dense clustering among the volatilities of North American and European indices, in contrast to the more dispersed patterns observed among Asian indices.

In Table 5 the estimated values of η are presented. Recall that $\eta_{i,j} = -\eta_{j,i}$. Together with α_i and α_j, $\eta_{i,j}$ determines the degree of asymmetry in the cross-covariance function, which is directly related to the time reversibility of the process. More specifically, when $H_{i,j} < 1$ (short-range interdependence) both the conditions $\alpha_i > \alpha_j$ and $\eta_{i,j} > 0$ result in a faster decrease of $\gamma_{i,j}(k)$ compared to $\gamma_{j,i}(k)$ as k increases. The values in $|\eta|$ range from 4×10^{-4}, for the pair SPX and KSE to 0.285 for KS11 and N225. Two-thirds of the 231 pairwise relationships are characterized by $|\eta_{i,j}| < 0.05$, and 90% of them by $|\eta_{i,j}| < 0.1$. High absolute values in η are estimated for pairs in which the Asian indices SSEC, N225, or AORD are involved. However, HSI, despite being in Asia, is characterized by small absolute $\eta_{i,j}$s. Among the lowest absolute values in η, we observe 5×10^{-4} for GDAXI and BSESN and 0.002 between FCHI and FTSE. These pairs are also characterized by similar α_i and α_j in Table 3, suggesting symmetric cross-covariances. Generally, interconnected exchanges, such as European and North American ones, show smaller absolute values in η. Overall, the optimization significantly increased the absolute values of the initial estimates obtained with the 2-step procedure, for both η and ρ.

The coherency constraint ensuring the positive semidefiniteness of the covariance matrix (cf. Section 2) was not directly included in the optimization routine. However, it was satisfied for 230 out of 231 pairs, with the exception of the pair FCHI-S5E, where the constraint was slightly exceeded, $c(H_i, H_j, \rho_{i,j}, \eta_{i,j}) = 1.04 > 1$.

	S5E	SSMI	IBEX	GDAXI	FTSE	FCHI	BFX	AEX	SSEC	NSEI	N225	KSE	KS11	HSI	BSESN	AORD	SPX	RUT	MXX	IXIC	DJI	BVSP
S5E	1																					
SSMI	0.923	1																				
	(0.508)																					
IBEX	0.868	0.745	1																			
	(0.579)	(0.555)																				
GDAXI	0.972	0.889	0.760	1																		
	(0.719)	(0.627)	(0.608)																			
FTSE	0.926	0.927	0.829	0.875	1																	
	(0.603)	(0.420)	(0.401)	(0.480)																		
FCHI	0.996	0.918	0.882	0.955	0.942	1																
	(0.691)	(0.642)	(0.724)	(0.716)	(0.499)																	
BFX	0.920	0.891	0.859	0.869	0.937	0.936	1															
	(0.565)	(0.551)	(0.608)	(0.594)	(0.425)	(0.721)																
AEX	0.978	0.948	0.804	0.956	0.941	0.969	0.934	1														
	(0.647)	(0.632)	(0.682)	(0.688)	(0.491)	(0.843)	(0.699)															
SSEC	0.245	0.339	0.167	0.209	0.325	0.252	0.243	0.263	1													
	(0.076)	(0.045)	(0.041)	(0.058)	(0.072)	(0.071)	(0.70)	(0.078)														
NSEI	0.434	0.544	0.242	0.417	0.498	0.417	0.439	0.460	0.455	1												
	(0.115)	(0.103)	(0.041)	(0.58)	(0.72)	(0.71)	(0.70)	(0.78)	(0.)													
N225	0.654	0.682	0.507	0.663	0.648	0.637	0.544	0.647	0.183	0.433	1											
	(0.173)	(0.155)	(0.135)	(0.154)	(0.168)	(0.160)	(0.141)	(0.161)	(0.164)	(0.102)												
KSE	0.019	0.043	-0.124	0.070	0.067	0.024	0.014	0.037	0.104	0.227	0.040	1										
	(0.000)	(0.001)	(-0.001)	(-0.031)	(0.044)	(-0.025)	(0.013)	(-0.010)	(-0.006)	(-0.005)	(-0.019)											
KS11	0.514	0.549	0.282	0.632	0.578	0.551	0.493	0.570	0.170	0.446	0.571	0.256	1									
	(0.095)	(0.127)	(0.109)	(0.107)	(0.083)	(0.125)	(0.118)	(0.116)	(0.117)	(0.082)	(0.256)	(0.015)										
HSI	0.580	0.615	0.485	0.635	0.680	0.630	0.618	0.645	0.355	0.512	0.560	0.016	0.680	1								
	(0.141)	(0.121)	(0.122)	(0.133)	(0.130)	(0.156)	(0.142)	(0.169)	(0.262)	(0.122)	(0.236)	(0.037)	(0.263)									
BSESN	0.433	0.464	0.258	0.505	0.501	0.467	0.409	0.472	0.297	0.894	0.569	0.299	0.699	0.636	1							
	(0.116)	(0.116)	(0.136)	(0.110)	(0.091)	(0.133)	(0.143)	(0.154)	(0.079)	(0.797)	(0.094)	(0.015)	(0.087)	(0.154)								
AORD	0.636	0.692	0.683	0.538	0.772	0.686	0.742	0.671	0.391	0.394	0.450	-0.019	0.284	0.541	0.331	1						
	(0.139)	(0.096)	(0.090)	(0.105)	(0.177)	(0.096)	(0.102)	(0.101)	(0.071)	(0.058)	(0.231)	(0.028)	(0.068)	(0.203)	(0.068)							
SPX	0.875	0.849	0.714	0.866	0.889	0.883	0.835	0.888	0.269	0.514	0.689	0.113	0.661	0.708	0.593	0.648	1					
	(0.353)	(0.307)	(0.316)	(0.364)	(0.342)	(0.370)	(0.314)	(0.367)	(0.025)	(0.029)	(0.081)	(0.014)	(0.086)	(0.089)	(0.039)	(-0.012)						
RUT	0.627	0.633	0.596	0.487	0.714	0.627	0.671	0.631	0.325	0.585	0.401	0.009	0.289	0.521	0.350	0.743	0.717	1				
	(0.194)	(0.180)	(0.193)	(0.215)	(0.207)	(0.224)	(0.195)	(0.230)	(0.034)	(0.014)	(0.050)	(-0.001)	(0.032)	(0.066)	(0.028)	(0.002)	(0.627)					
MXX	0.517	0.539	0.517	0.457	0.689	0.570	0.590	0.537	0.279	0.486	0.445	0.052	0.408	0.608	0.474	0.719	0.648	0.710	1			
	(0.274)	(0.192)	(0.195)	(0.235)	(0.269)	(0.229)	(0.180)	(0.220)	(0.012)	(0.017)	(0.073)	(0.014)	(0.064)	(0.060)	(0.011)	(0.003)	(0.427)	(0.249)				
IXIC	0.759	0.718	0.592	0.802	0.782	0.779	0.726	0.791	0.108	0.352	0.655	0.160	0.700	0.724	0.617	0.511	0.913	0.573	0.586	1		
	(0.316)	(0.302)	(0.308)	(0.341)	(0.257)	(0.350)	(0.288)	(0.364)	(0.026)	(0.060)	(0.003)	(0.051)	(0.047)	(0.025)	(0.057)	(0.717)	(0.663)	(0.242)	(0.)			
DJI	0.873	0.862	0.700	0.869	0.892	0.878	0.835	0.894	0.280	0.507	0.688	0.101	0.670	0.702	0.573	0.645	0.989	0.696	0.629	0.896	1	
	(0.339)	(0.294)	(0.298)	(0.349)	(0.339)	(0.350)	(0.300)	(0.334)	(0.019)	(0.022)	(0.077)	(0.013)	(0.087)	(0.089)	(0.026)	(-0.033)	(0.925)	(0.564)	(0.443)	(0.592)		
BVSP	0.639	0.672	0.466	0.634	0.685	0.640	0.591	0.672	0.311	0.701	0.628	-0.046	0.609	0.628	0.606	0.490	0.712	0.578	0.501	0.633	0.714	1
	(0.188)	(0.180)	(0.168)	(0.204)	(0.144)	(0.196)	(0.154)	(0.199)	(0.020)	(0.023)	(0.039)	(-0.014)	(0.012)	(0.012)	(0.014)	(0.012)	(0.309)	(0.272)	(0.239)	(0.350)	(0.271)	

Table 4: Estimates of $\rho_{i,j}$ on $\log\left(100\sqrt{RV \times 252}\right)$, where RV is the realized variance from Oxford-Man (rv5). The MDE estimates are shown above and the initial values from the 2-step procedure are shown below among parentheses. The MDE procedure uses $\mathcal{L} = \{0,\ 1,\ 2,\ 3,\ 4,\ 5,\ 20,\ 50\}$ and $\Delta = 1/252$. The 2-step procedure relies on the Low frequency estimator from Dugo et al. (2024) with time-lag equal to 1 and univariate parameters from Table 3. Symbol is based on the provider convention.

	S5E	SSMI	IBEX	GDAXI	FTSE	FCHI	BFX	AEX	SSEC	NSEI	N225	KSE	KS11	HSI	BSESN	AORD	SPX	RUT	MXX	IXIC	DJI	BVSP
S5E	0																					
SSMI	-0.027	0																				
	(0.021)																					
IBEX	0.008	0.025	0																			
	(0.007)	(-0.022)																				
GDAXI	0.008	0.044	0.011	0																		
	(0.017)	(-0.016)	(0.007)																			
FTSE	0.010	0.055	0.034	0.003	0																	
	(-0.006)	(-0.017)	(0.000)	(-0.014)																		
FCHI	0.019	0.050	0.027	0.009	0.002	0																
	(0.015)	(-0.022)	(0.004)	(0.000)	(0.012)																	
BFX	-0.014	-0.018	-0.010	-0.028	-0.049	-0.044	0															
	(0.010)	(-0.008)	(0.011)	(0.005)	(0.008)	(0.003)																
AEX	0.004	0.030	0.012	-0.004	-0.020	-0.017	0.027	0														
	(0.020)	(-0.014)	(0.006)	(0.006)	(0.016)	(0.007)	(0.003)															
SSEC	0.073	0.203	-0.117	-0.072	-0.092	-0.097	-0.138	-0.096	0													
	(-0.011)	(-0.008)	(0.004)	(0.014)	(0.011)	(0.016)	(0.007)	(0.012)														
NSEI	-0.027	-0.003	0.085	0.063	0.023	0.031	0.028	0.019	0.210	0												
	(-0.051)	(-0.061)	(0.041)	(0.053)	(0.037)	(0.049)	(0.043)	(0.061)	(-0.013)													
N225	-0.090	-0.041	0.094	0.104	0.099	0.098	0.064	0.081	-0.088	-0.074	0											
	(-0.074)	(-0.083)	(0.065)	(0.064)	(0.057)	(0.073)	(0.052)	(0.074)	(-0.023)	(-0.004)												
KSE	0.052	0.028	-0.117	0.002	-0.040	-0.049	-0.076	-0.047	0.123	-0.087	0.060	0										
	(0.030)	(0.015)	(-0.050)	(-0.028)	(0.007)	(-0.041)	(-0.027)	(-0.037)	(-0.011)	(-0.004)	(0.001)											
KS11	0.001	0.131	-0.045	0.023	-0.031	-0.016	-0.039	-0.031	0.050	-0.050	0.285	0.184	0									
	(-0.016)	(-0.027)	(0.023)	(0.026)	(0.009)	(0.023)	(0.023)	(0.021)	(-0.031)	(0.009)	(0.037)	(0.007)										
HSI	-0.012	0.039	-0.003	0.027	0.041	0.020	0.002	-0.011	0.084	0.009	0.115	0.037	-0.001	0								
	(-0.017)	(-0.020)	(-0.015)	(0.016)	(0.027)	(0.025)	(0.021)	(0.025)	(0.032)	(0.021)	(0.047)	(0.004)	(0.011)									
BSESN	0.029	0.024	0.031	-0.001	0.006	0.028	-0.022	-0.024	0.032	-0.050	0.150	0.093	0.095	0.018	0							
	(-0.058)	(-0.071)	(-0.051)	(-0.061)	(-0.047)	(-0.060)	(0.054)	(0.075)	(-0.006)	(-0.013)	(0.002)	(0.009)	(-0.012)	(-0.024)								
AORD	-0.079	-0.080	-0.074	-0.088	-0.138	-0.112	-0.090	0.093	-0.208	-0.093	0.006	-0.049	-0.160	-0.101	-0.104	0						
	(-0.074)	(-0.064)	(-0.042)	(-0.066)	(-0.075)	(-0.052)	(-0.037)	(0.061)	(-0.019)	(-0.020)	(-0.004)	(-0.024)	(-0.027)	(-0.132)	(-0.021)							
SPX	0.015	0.050	-0.030	-0.009	-0.027	-0.002	-0.045	-0.015	-0.093	0.002	-0.116	0.000	- 0.031	-0.034	0.023	-0.134	0					
	(0.094)	(0.067)	(-0.086)	(-0.066)	(-0.102)	(-0.075)	(-0.086)	(-0.087)	(0.007)	(-0.084)	(-0.124)	(-0.004)	(-0.038)	(-0.054)	(-0.097)	(-0.124)						
RUT	-0.017	-0.040	0.033	0.039	0.029	0.035	0.027	0.027	-0.132	0.067	-0.003	0.077	0.093	0.012	0.042	-0.092	-0.035	0				
	(0.099)	(0.065)	(-0.071)	(-0.068)	(-0.098)	(-0.076)	(-0.086)	(-0.091)	(0.006)	(-0.079)	(-0.095)	(-0.019)	(-0.061)	(-0.057)	(-0.091)	(-0.105)	(0.032)					
MXX	0.020	0.037	-0.031	-0.017	-0.008	-0.017	-0.016	-0.024	-0.098	-0.046	0.094	-0.004	0.081	-0.026	0.059	-0.099	-0.005	0.018	0			
	(0.033)	(0.038)	(-0.040)	(-0.029)	(-0.031)	(-0.034)	(-0.036)	(-0.040)	(-0.002)	(0.063)	(0.052)	(0.013)	(-0.024)	(-0.030)	(-0.061)	(-0.089)	(-0.035)	(-0.046)				
IXIC	0.035	0.058	-0.038	-0.025	-0.030	-0.018	-0.040	-0.031	-0.147	0.048	0.111	-0.001	0.049	-0.030	0.016	-0.105	0.026	0.042	-0.003	0		
	(0.110)	(0.086)	(-0.090)	(-0.081)	(-0.114)	(-0.091)	(-0.095)	(-0.105)	(0.018)	(0.105)	(0.129)	(0.008)	(0.060)	(-0.051)	(-0.124)	(-0.099)	(0.020)	(-0.013)	(0.034)			
DJI	0.004	0.039	0.017	-0.004	0.014	-0.008	-0.033	-0.004	-0.082	-0.005	0.110	-0.010	0.021	0.030	0.028	-0.122	-0.012	0.032	-0.004	-0.035	0	
	(0.075)	(0.049)	(0.072)	(0.048)	(0.084)	(0.056)	(-0.070)	(-0.068)	(0.011)	(0.077)	(0.102)	(0.003)	(0.024)	(0.049)	(-0.085)	(-0.126)	(-0.012)	(-0.035)	(0.033)	(-0.031)		
BVSP	-0.038	-0.049	-0.022	-0.079	-0.052	-0.054	0.032	0.038	0.055	-0.076	0.074	0.064	-0.016	-0.046	0.050	-0.070	-0.027	0.037	-0.025	-0.017	-0.020	0
	(0.036)	(0.005)	(0.030)	(0.016)	(0.024)	(0.021)	(-0.029)	(-0.023)	(-0.002)	(0.040)	(0.043)	(-0.031)	(-0.002)	(0.001)	(-0.047)	(0.031)	(-0.053)	(-0.054)	(-0.019)	(-0.070)	(-0.045)	

Table 5: Estimates of $\eta_{i,j}$ on $\log\left(100\sqrt{RV \times 252}\right)$, where RV is the realized variance from Oxford-Man (rv5). The MDE estimates are shown above and the initial values from the 2-step procedure are shown below among parentheses. The MDE procedure uses $\mathcal{L} = \{0,\ 1,\ 2,\ 3,\ 4,\ 5,\ 20,\ 50\}$ and $\Delta = 1/252$. The 2-step procedure relies on the Low frequency estimator from Dugo et al. (2024) with time-lag equal to 1 and univariate parameters from Table 3. Symbol is based on the provider convention.

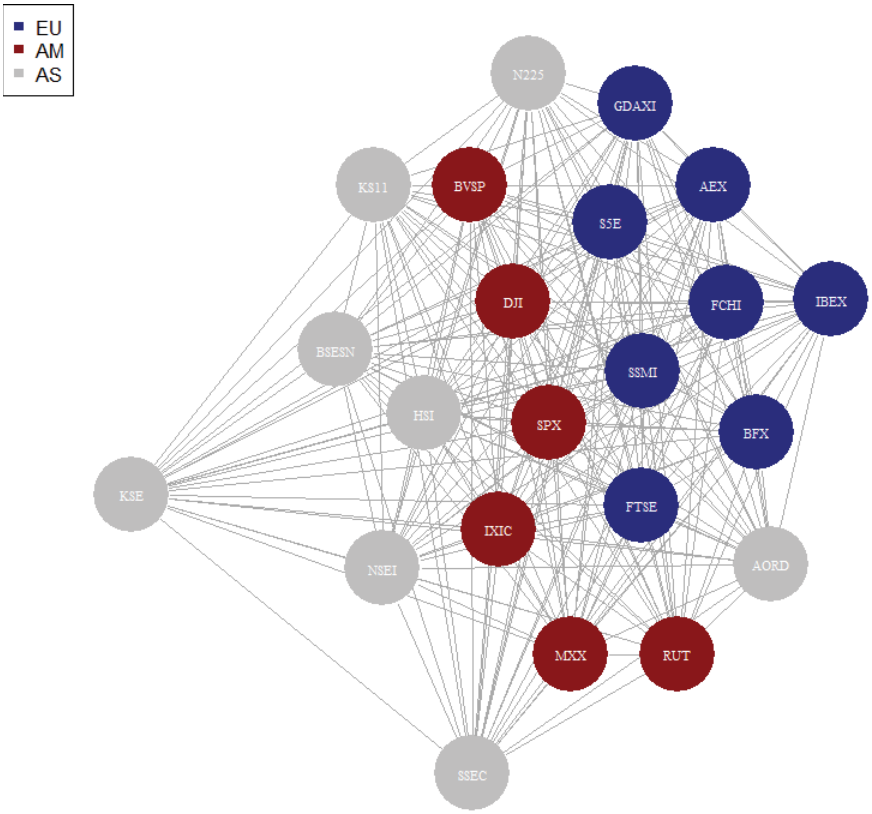

Figure 3: Undirected graph representation of the estimates of $\rho_{i,j}$, $i, j = 1, \ldots, N$, $i \neq j$. The nodes correspond to indices and the edges among pairs of indices have length inversely proportional to the MDE estimates of $\rho_{i,j}$ reported in Table 4.

To demonstrate the goodness of fit of our model and illustrate the degrees of asymmetry in the empirical cross-covariances of log-volatility, in Figure 4 we present plots for the pairs FCHI-FTSE and KS11-N225, two extreme cases, identified based on the values of $|\eta_{i,j}|$: when the value of the former is among the lowest ones and when it is the highest. Note that the asymmetry depends also on α_i and α_j.

In the FCHI - FTSE case, we have $\eta_{i,j} = 0.002$, $\alpha_i = 1.316$, and $\alpha_j = 1.446$. The strong symmetry suggested by the close values of α_i and α_j and the small $\eta_{i,j}$ is supported empirically. In the KS11 - N225 case, where $\eta_{i,j} = 0.285$, $\alpha_i = 2.004$, and $\alpha_j = 1.768$, we expect and indeed observe asymmetry. In this instance, since $H_{i,j} < 1$, both $\eta_{i,j} > 0$ and $\alpha_i > \alpha_j$ accelerate the right-hand side of the cross-covariance towards zero.[2] In the former case, $\eta_{i,j} > 0$ and $\alpha_i < \alpha_j$ compensate each other.

Our model fits well both these different behaviors. Moreover, as shown in Appendix C, it effectively fits the autocovariance of the marginal components. The fit is also good for auto and cross-covariances of all the 22 components in the system, which overall exhibit characteristics closer to the symmetric case (see Online Appendix for further empirical evidence).

5.2 Slow mean reversion

Following an approach similar to Gatheral et al. (2018), we examine the empirical cross-covariance against $k^{H_i+H_j}$, where H_i and H_j are proxied by the estimated values in Table 3. According to the cross-covariance function of the mfOU process in the small α (or small k) regime, this relationship should be approximately linear. Figure 5 shows that this linear behavior holds for lags up to 50, particularly well in the symmtric case of FCHI-FTSE. Evidence for autocovariances is provided in Appendix C, with similar findings observed across

[2]The opposite holds when $\eta_{i,j} < 0$ and/or $\alpha_i < \alpha_j$

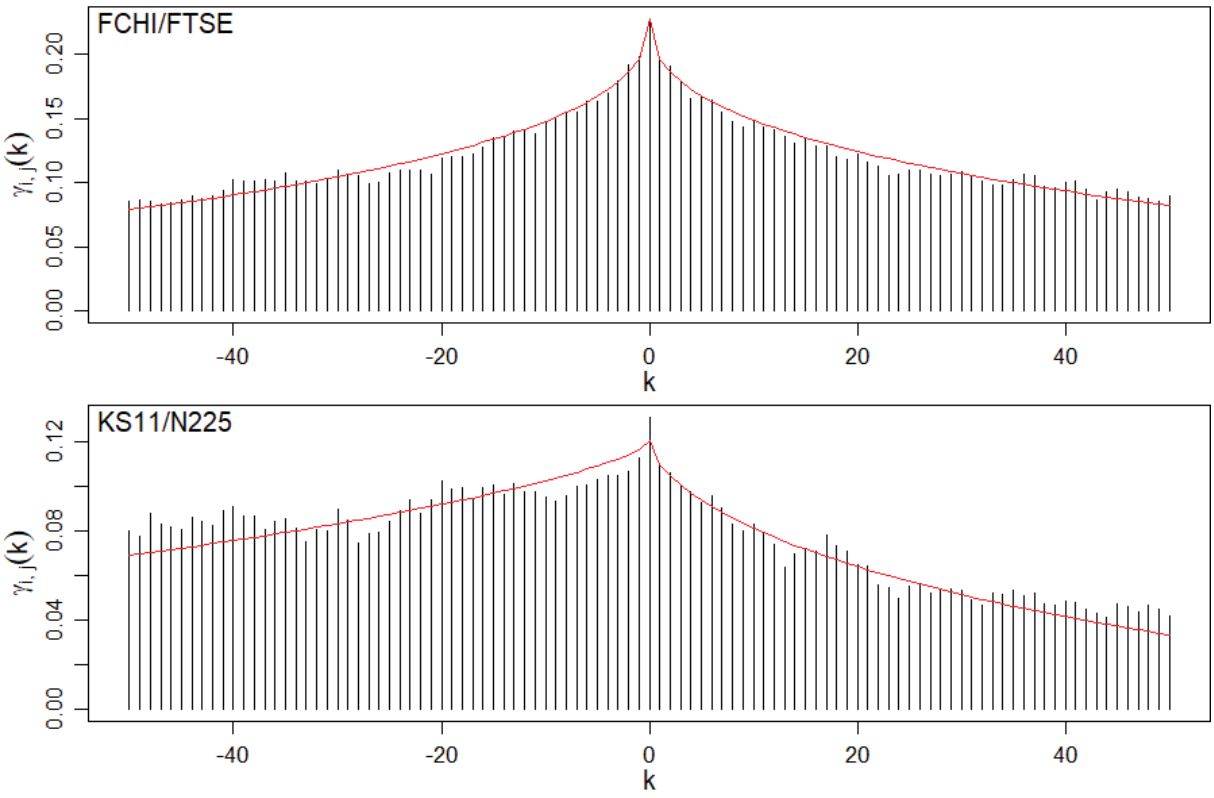

Figure 4: Empirical cross-covariances of log-volatilities as bars, alongside the theoretical cross-covariances from our model, indicated by the red curves and based on the estimated parameters from Tables 3, 4, and 5. The upper panel shows the pair FCHI-FTSE, while the lower panel shows the pair KS11-N225.

the entire system available in the Online Appendix. Motivated by these findings, we attempt estimation of the

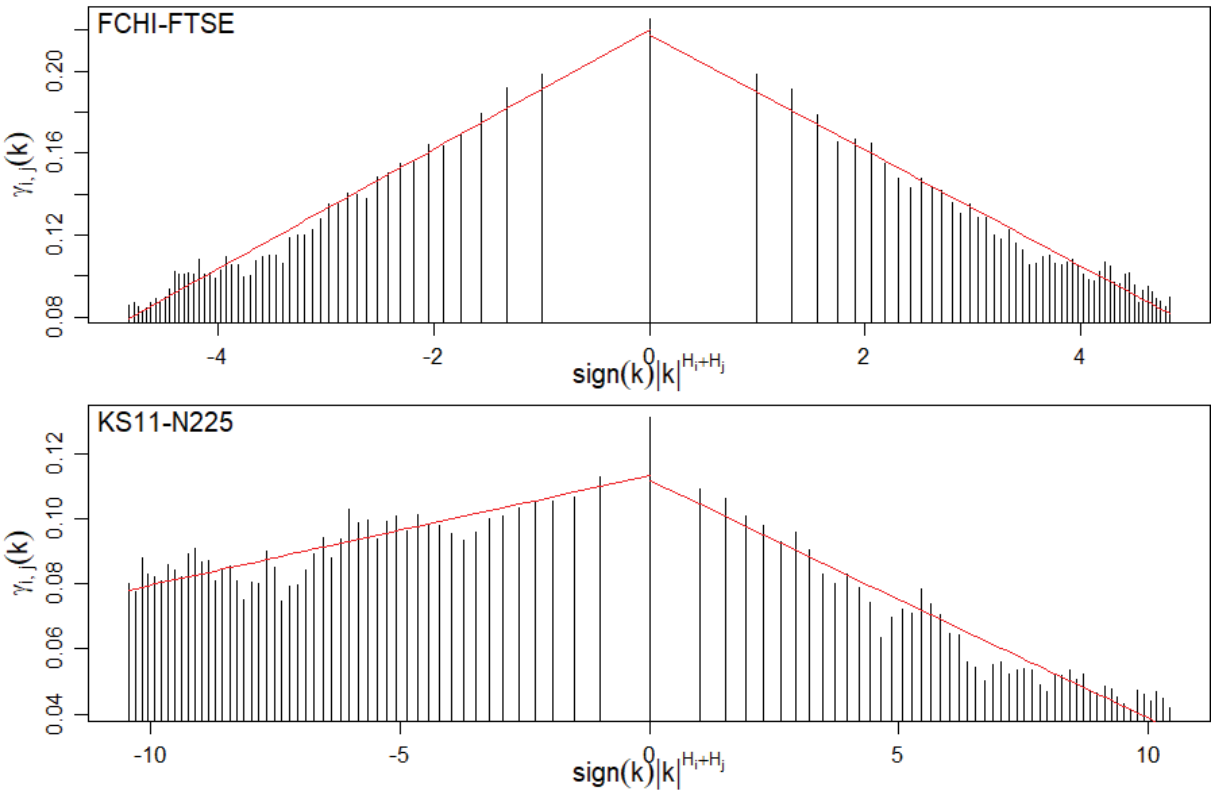

Figure 5: Empirical cross-covariances of log-volatilities as bars, plotted against a suitable power of the lag (given by the sum of the Hurst exponents), alongside the best linear fits, indicated by the red lines. The upper panel shows the pair FCHI-FTSE, while the lower panel shows the pair KS11-N225.

system using the asymptotic cross-covariance function given in Proposition 2 in the moment conditions of the MDE estimator. The resulting fit is strong, as demonstrated in Figure 6. Additional evidence on univariate marginals is provided in Appendix C, with findings on the remaining series available in the Online Appendix. Parameter variations were minor for the FCHI-FTSE pair but more significant for N225-KS11. Overall, cross-covariances between the two estimation procedures are consistent, a direct result of the MDE design, though the estimated parameters can vary (cf. Online Appendix). This can be interpreted as additional evidence for the "near non-stationary regime" of realized volatility found by Gatheral et al. (2018).

6 Spillovers

Prompted by the asymmetries in the cross-covariances, we study the effects of the lead-lag relationship in the framework of spillovers (Diebold and Yilmaz 2009; Diebold and Yilmaz 2012). Spillovers are defined in a multivariate system of time series as the shares of the forecast error variance in one variable due to the effect of the innovations in another variable. Let $\psi_{i,j}(h)$, be the share of the variance in the error of predicting Y^i_{t+h} due to innovations in the variable $\left(Y^j_s\right)_{s\in[t,t+h]}$, for $i,j=1,\ldots,N$. In Pesaran (1997) and Pesaran and Shin (1998), in the discrete time setting, this is defined as

$$\psi_{i,j}(h)=\frac{\mathbb{E}\left[\left(Y^i_{t+h}-\mathbb{E}\left[Y^i_{t+h}|\mathcal{F}_{t-1}\right]\right)^2\right]-\mathbb{E}\left[\left(Y^i_{t+h}-\mathbb{E}\left[Y^i_{t+h}|\mathcal{F}_{t-1},\left(\varepsilon^j_{t+k}\right)_{k=0}^{h}\right]\right)^2\right]}{\mathbb{E}\left[\left(Y^i_{t+h}-\mathbb{E}\left[Y^i_{t+h}|\mathcal{F}_{t-1}\right]\right)^2\right]},$$

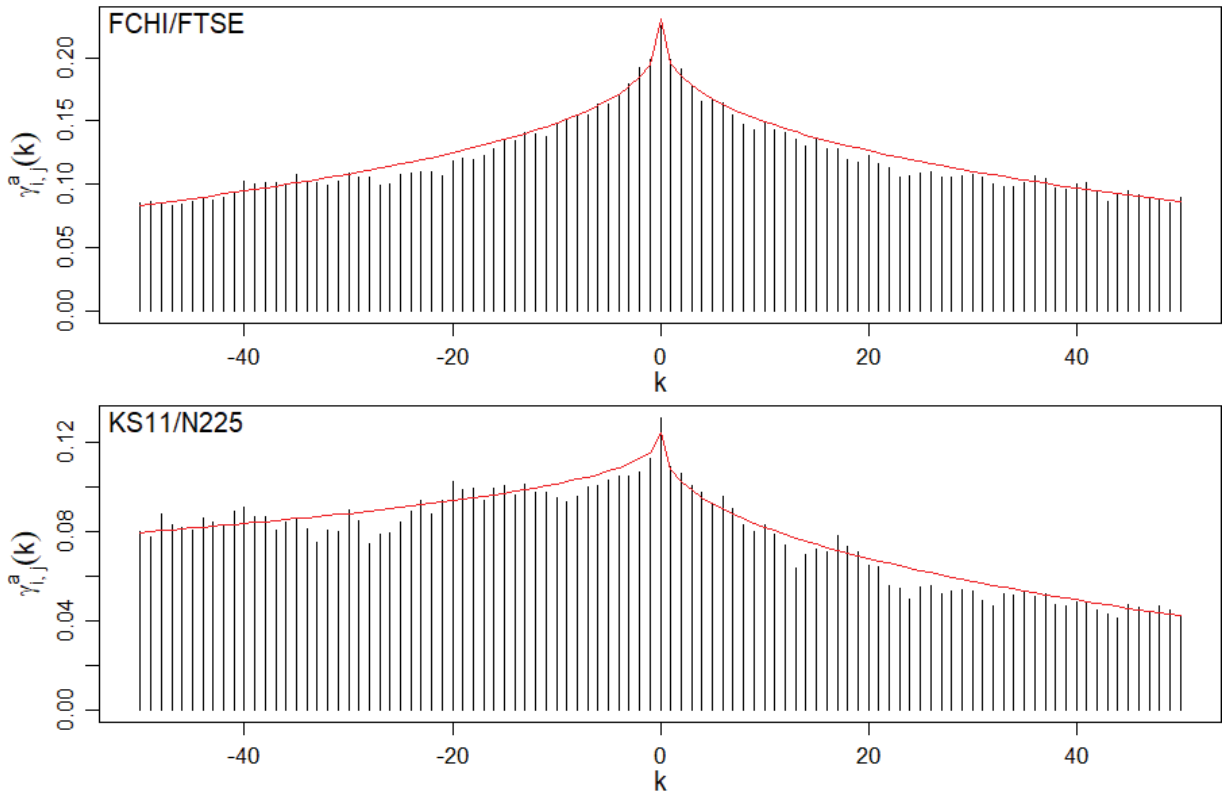

Figure 6: Empirical cross-covariances of log-volatilities as bars, alongside the approximate theoretical cross-covariances from our model for $\alpha \to 0$, indicated by the red curves and based on the estimated parameters (available in the Online Appendix). The upper panel shows the pair FCHI-FTSE, while the lower panel shows the pair KS11-N225.

where ε_t is the N-variate white noise innovation in Y_t at time t, ε_t^j is its j-th component, and $\mathcal{F}_{t-1}$ is the information set at time $t-1$, i.e. the filtration generated by the underlying $\varepsilon_{t-i},\ i=1,\ldots$. In order to use the information in the variance decomposition matrix Ψ, with entries $[\Psi(h)]_{i,j}=\psi_{i,j}(h)$, to construct spillover indices in the presence of correlated white noises, Diebold and Yilmaz (2012) consider the normalized quantities

$$\widetilde{\psi}_{i,j}(h)=\frac{\psi_{i,j}(h)}{\sum_{j=1}^{N}\psi_{i,j}(h)}. \tag{5}$$

The mfOU process admits an integral moving average representation where the innovations are white noise (cf. Dugo et al. 2024). In order to give a meaningful intepretation to time, and spillovers, we need to restrict our attention to the causal version of the mfOU process, that is, when the process depends only on past values of the driving white noise (see Amblard et al. 2010 for details). In this setting, we lose one degree of freedom in the choice of the parameters, which we can see as fixing $\eta_{i,j}=f(H_i,H_j,\rho_{i,j})$ for a function f given in Amblard et al. (2010). In this setting, $\eta_{i,j}=0 \iff H_i=H_j$.

Proposition 4. *In the adapted time discretization of the causal mfOU process (see (15)), assuming $t>h$, we have*

$$\widetilde{\psi}_{i,j}(h)=\frac{G_{i,j}^2/\sqrt{G_{j,j}}}{\sum_{k=1}^{N}G_{i,k}^2/\sqrt{G_{k,k}}},$$

where

$$G_{i,j}=\sqrt{\frac{B(H_i+\frac{1}{2},H_i+\frac{1}{2})B(H_j+\frac{1}{2},H_j+\frac{1}{2})}{\sin(\pi H_i)\sin(\pi H_j)}}\frac{1}{B(H_i+\frac{1}{2},H_j+\frac{1}{2})}\frac{\sin(\pi(H_i+H_j))}{(\cos(\pi H_i)+\cos(\pi H_j))}\rho_{i,j},$$

and $B(x,y),\ x,y>0$, denotes the Beta function.

The proof is given in Appendix E.

Remark 2. *In the adapted discretization of the moving average representation of the causal mfOU process, the forecast error variance shares, $\widetilde{\psi}_{i,j}$, and the resulting spillover indices are independent of the forecasting horizon, h, the history of the process, $\mathcal{F}_{t-1}$, and the discretization step.*

We proceed to estimate the causal model following the same methodology detailed in Section 3 with the additional constraint $\eta_{i,j}=f(H_i,H_j,\rho_{i,j})$, calculate $\widetilde{\psi}_{i,j}$ with the estimated parameters, and construct the spillover indices defined in Table 6.[3] We obtain the following results over the whole period from January 2000 to June 2022.

- *Total spillovers* amount to 85% of the normalized forecast error variance decomposition of log-volatilities.
- *Directional spillovers* are illustrated in Figure 7. The top panel shows that the amount of received spillovers is quite uniform among European and North American volatilities, with greater differences among other components. Their level of variability is a direct consequence of the normalization step in (5). Greater variability is preserved in the spillovers transmitted to others, in the middle panel, resulting in clearly different net quantities. In fact, as shown in the bottom panel, European and North American indices generally transmit at least as much volatility spillover as they receive, with FTSE, DJI, and SPX playing major roles, while Asian indices consistently exhibit negative net volatility spillovers. An exception in Europe is IBEX, which shows negative net volatility spillovers. The KSE index appears to be the most isolated in our sample in terms of volatility, with relatively low levels of both transmitted and received spillovers.
- *Net pairwise spillovers*, presented in Figure 8, offer a more detailed perspective. Although this measure cannot be interpreted in terms of shares of the normalized forecast error variance, net pairwise spillovers provide valuable qualitative insights. Notably, FTSE is the only index with all positive net pairwise volatility spillovers, followed by SPX, which only exhibits negative net volatility spillovers against FTSE. Other primary net transmitters include DJI and AEX. The main net receivers appear to be

[3]Estimates obtained in the causal setting are available in the Online Appendix.

Table 6: Definitions of Spillover Indices from Diebold and Yilmaz (2012), where $\widetilde{\psi}_{i,j}(h)$ is defined in (5).

Spillover Index	**Description**	**Definition**
Total	Aggregation over all components in the system of the normalized forecast error variances due to shocks to other components.	$S(h) = \frac{\sum_{i,j=1, i\neq j}^{N} \widetilde{\psi}_{ij}(h)}{N} \cdot 100$
Received	Share of total spillovers received by a particular component of the system from the other components.	$S_{i,\cdot}(h) = \frac{\sum_{j=1, j\neq i}^{N} \widetilde{\psi}_{ij}(h)}{N} \cdot 100$
Transmitted	Share of total spillovers transmitted by a particular component of the system to the other components.	$S_{\cdot,i}(h) = \frac{\sum_{j=1, j\neq i}^{N} \widetilde{\psi}_{ji}(h)}{N} \cdot 100$
Net	Difference between the spillovers transmitted to and those received from all other components of the system.	$S_i(h) = S_{\cdot,i}(h) - S_{i,\cdot}(h)$
Net Pairwise	Difference between the spillovers transmitted from component i to component j and those transmitted from j to i.	$S_{i,j}(h) = \left(\frac{\widetilde{\psi}_{ji}(h) - \widetilde{\psi}_{ij}(h)}{N} \right) \cdot 100$

SSEC and KSE, with the latter being relatively neutral and primarily influenced by the geographically neighbouring BSESN and NSEI indices.

The presence of substantial spillovers suggests that forecasting volatility time series as a multivariate system could provide benefits. In the context of the mfOU process, this task could be easily achieved using rules for conditional expectations of Gaussian vectors (as, for example, in Bennedsen et al. 2021).

7 Conclusion

Motivated by recent advances in volatility modeling, we introduce a multivariate model for rough volatility. Our objective is to extend the widely-used RFSV model of Gatheral et al. (2018) to a multivariate framework and empirically study a system of historical volatilities. This extension retains consistency with the findings in the univariate case, namely that volatility is rough and mean reverts slowly, while broadening our understanding of volatility dynamics through the analysis of cross-covariances and spillover effects, which are descriptive of how volatility evolves across markets. These results can have implications in risk management and forecasting techniques in finance.

The results in this paper could be further developed considering the distinction between spot and realized volatility, for example leveraging the moment structure of integrated variance (as in Bolko et al. 2023) or directly estimating spot volatility (Jacod 2000). Another potential direction is to extend the empirical study with rolling window parameter estimation, which could then be used for dynamic forecasting and spillover analyses.

In conclusion, by introducing the multivariate fractional Ornstein-Uhlenbeck process, we confirm the increasing evidence that rough processes effectively model volatility dynamics and extend our understanding of these dynamics to a multidimensional context, with potential for further applications.

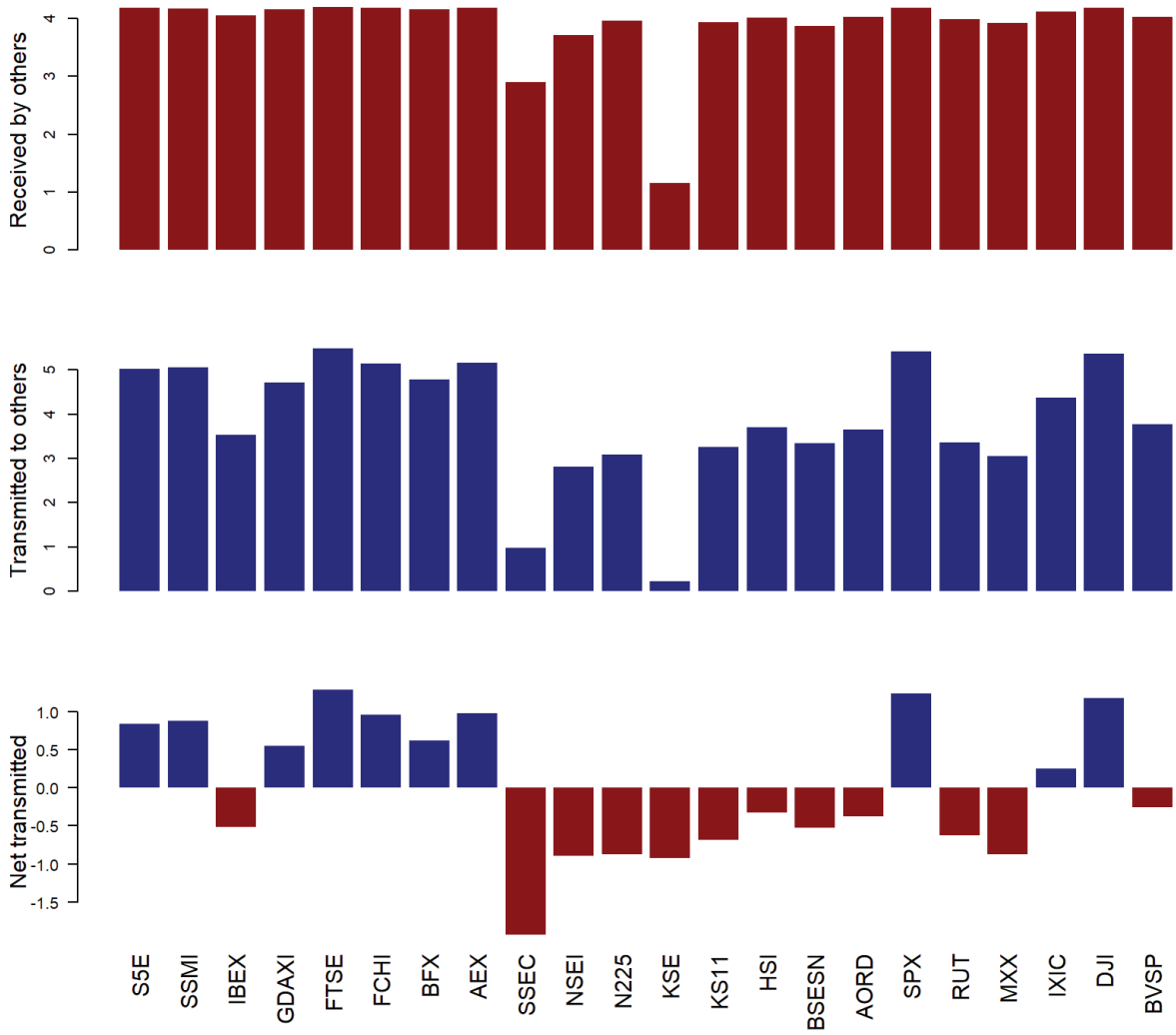

Figure 7: Estimates of directional volatility spillovers over the whole period (2000-2022) for each index. The figures in the first and second rows represent aggregated shares of the forecast error variance decomposition. See definitions in Table 6.

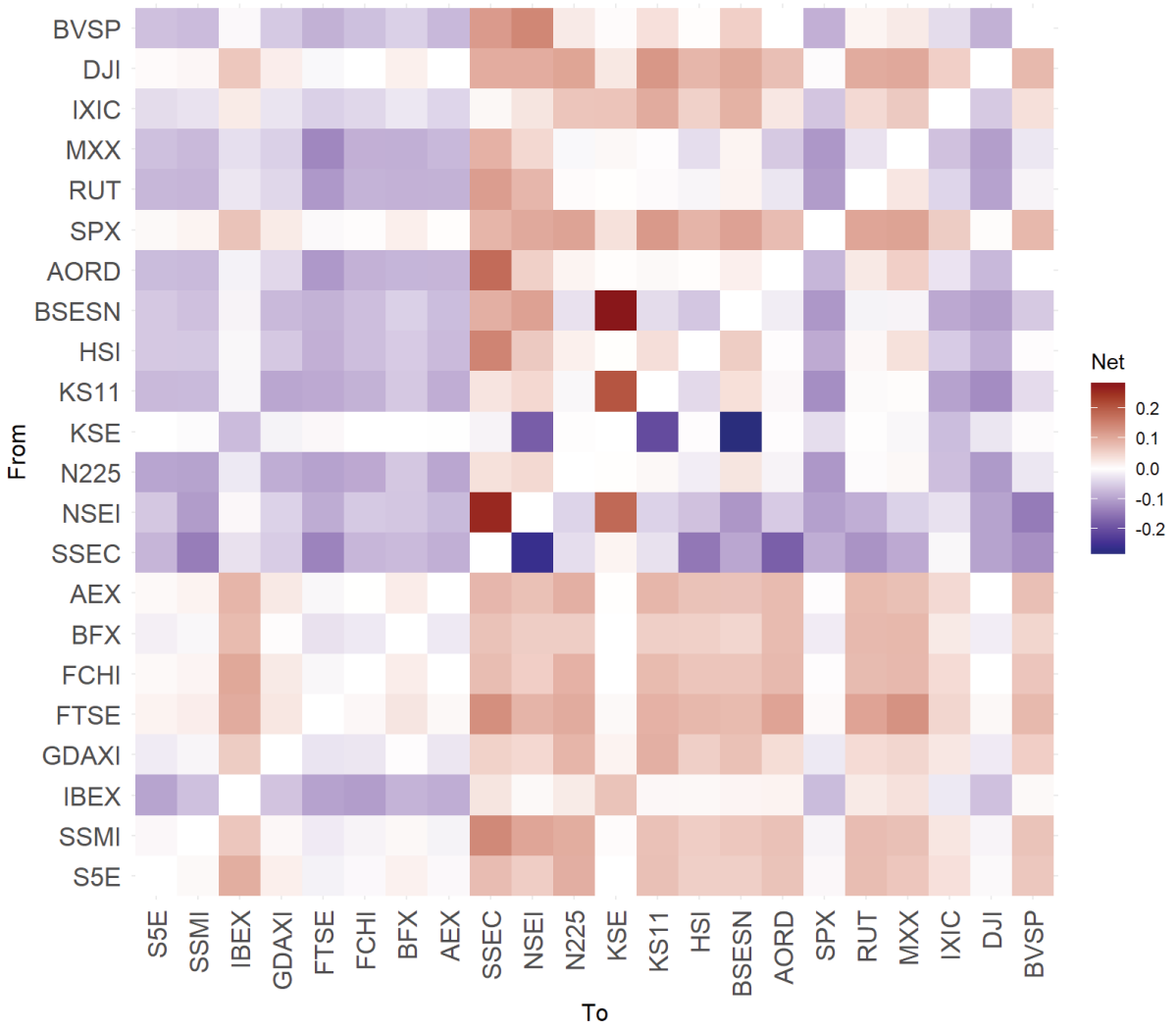

Figure 8: Estimates of net pairwise volatility spillovers over the whole period (2000-2022) for each combination of indices i,j. It is the difference between the volatility shocks transmitted from index i to index j and those transmitted from j to i. See definition in Table 6.

A Asymptotic theory for the MDE estimator

Proof of Proposition 3 - (I): By definition of the MDE estimator, $\hat{\theta}$ satisfies the first order condition

$$\nabla \mathcal{T}(\theta)\,|_{\theta=\hat{\theta}} = 0,$$

where $\nabla \mathcal{T}(\theta)$ denotes the gradient of $\mathcal{T}(\theta)$.Using a first-order Taylor expansion around θ_0, the true value of the parameter, with Lagrange form of the remainder, we have

$$\nabla \mathcal{T}(\theta)_{\theta=\hat{\theta}} = \nabla \mathcal{T}(\theta)\,|_{\theta=\theta_0} + \nabla^2 \mathcal{T}(\theta)\,|_{\theta=\theta^\star}\left(\hat{\theta}-\theta_0\right) = 0,$$

where $\theta^\star$ lies between θ_0 and $\hat{\theta}$, and $\nabla^2 \mathcal{T}(\theta)$ indicates the Hessian of $\mathcal{T}(\theta)$. Solving for $\hat{\theta}-\theta_0$, we get

$$\hat{\theta}-\theta_0 = -\left(\nabla^2 \mathcal{T}(\theta)\right)^{-1}|_{\theta=\theta^\star} \nabla \mathcal{T}(\theta)\,|_{\theta=\theta_0}. \tag{6}$$

Given the differentiability of $\gamma^k_{i,j}(\theta)$ when $H_{i,j} \neq 1$, we can explicitly calculate the terms in (6) as

$$\nabla \mathcal{T}(\theta) = -2J_\gamma^T W_n \left(\hat{\gamma}_n - \gamma(\theta)\right), \tag{7}$$

and

$$\nabla^2 \mathcal{T}(\theta) = 2J_\gamma^T W_n J_\gamma + o\left(\hat{\gamma}_n - \gamma(\theta)\right), \tag{8}$$

where J_γ is the Jacobian matrix of $\gamma(\theta)$ and $o\left(\hat{\gamma}_n - \gamma(\theta)\right)$ represents a term containing the second derivatives of $\gamma(\theta)$, which are bounded in a neighborhood of $\hat{\theta}$, times $\hat{\gamma}_n - \gamma(\theta)$. Dugo et al. (2024) show that Y_t is ergodic and consequently that

$$\hat{\gamma}^k_{i,j} \xrightarrow{p} \gamma_{i,j}(k), \quad \text{as } n \to \infty,$$

which implies that

$$\hat{\gamma}_n \xrightarrow{p} \gamma(\theta) \quad as\ n \to \infty.$$

From this we can conclude that

$$\nabla \mathcal{T}(\theta) \xrightarrow{p} 0 \quad \text{and} \quad \nabla^2 \mathcal{T}(\theta) \xrightarrow{p} 2J_\gamma^T W J_\gamma. \tag{9}$$

These two convergences imply together that $\theta^\star \xrightarrow{p} \theta_0$ and $\hat{\theta} \xrightarrow{p} \theta_0$.
Proof of Proposition 3 - (II): In order to establish the central limit theorem for $\hat{\theta}$, we need to understand the limit distribution of the term in (7). It is possible to prove that when $H_i + H_j < \frac{3}{2}$, $i, j = 1, \ldots, N,\ \forall k$

$$\sqrt{n}\left(\frac{1}{n}\sum_{t=1}^{n-k} Y^i_{t+k} Y^j_t - \gamma_{i,j}(k)\right) \xrightarrow{d} N(0, \sigma^2_{ij}(k)), \tag{10}$$

where

$$\sigma^2_{ij}(k) = \mathrm{Var}\left(Y^i_{t+k} Y^j_t\right) + 2\sum_{s=0}^{\infty} \mathrm{Cov}\left(Y^i_{t+k} Y^j_t, Y^i_{t+k+s} Y^j_{t+k}\right).$$

The previous result can be extended to the vector $\hat{\gamma}_n - \gamma(\theta)$, as

$$\sqrt{n}\left(\hat{\gamma}_n - \gamma(\theta)\right) \xrightarrow{d} N(0, \Gamma), \tag{11}$$

where the diagonal elements of Γ would coincide with $\sigma^2_{ij}(k)$ above, $i, j = 1, \ldots, N,\ k \in \mathcal{L}$, and the additional off-diagonal covariance terms would be in a similar form. The results in (10) and (11) are deduced by Theorem 3.6 in Dugo et al. (2024). See also Theorem 4 in Arcones (1994). Therefore, it is possible to conclude that

$$\sqrt{n}\nabla \mathcal{T}(\theta) = -\sqrt{n}2J_\gamma^T W_n \left(\hat{\gamma}_n - \gamma(\theta)\right) \xrightarrow{d} N(0, 4J_\gamma^T W \Gamma W J_\gamma)$$

which together with (6), (9), and Slutsky's Theorem establishes (II).

Table 7: Description of the dataset utilized in the empirical analysis obtained from the Oxford-Man realized library. Log-volatilities are computed as $\log\left(100\sqrt{RV \times 252}\right)$. The columns Missing and Zeros report the count of days with missing values and zero volatility, respectively. Descriptive statistics include the in-sample average (Mean), standard deviation (SD), minimum (Min), median (Med), and maximum (Max) values. Included specifies wether the time series is included in the multivariate system under analysis or not.

Symbol	**Country**	**Count**		**Descriptive Statistics**					**Included**
		Missing	**Zeros**	**Mean**	**SD**	**Min**	**Median**	**Max**	
AEX	Netherlands	159	0	2.53	0.51	0.69	2.48	4.63	Yes
AORD	Australia	218	0	2.14	0.48	0.51	2.09	4.70	Yes
BFX	Belgium	161	0	2.46	0.47	1.16	2.42	4.57	Yes
BSESN	India	314	9	2.64	0.49	1.12	2.59	5.27	Yes
BVLG	Peru	3495	1	2.27	0.38	1.17	2.26	4.14	No
BVSP	Brazil	363	0	2.76	0.41	1.28	2.73	4.80	Yes
DJI	USA	264	0	2.44	0.56	0.79	2.41	4.99	Yes
FCHI	France	157	0	2.63	0.50	0.97	2.61	4.73	Yes
FTMIB	Italy	2579	0	2.60	0.45	0.33	2.59	4.42	No
FTSE	UK	226	0	2.54	0.50	0.61	2.48	5.10	Yes
GDAXI	Germany	196	0	2.68	0.52	1.17	2.64	4.80	Yes
GSPTSE	Canada	857	0	2.21	0.55	0.67	2.14	5.61	No
HSI	Hong Kong	389	0	2.54	0.42	1.20	2.49	4.65	Yes
IBEX	Spain	194	0	2.70	0.47	1.17	2.71	4.77	Yes
IXIC	USA	257	0	2.54	0.55	0.95	2.48	4.81	Yes
KS11	South Korea	362	0	2.54	0.51	0.61	2.48	4.81	Yes
KSE	Pakistan	416	0	2.47	0.52	-1.52	2.43	4.57	Yes
MXX	Mexico	257	0	2.40	0.45	1.10	2.35	4.74	Yes
N225	Japan	434	0	2.52	0.47	0.83	2.50	4.59	Yes
NSEI	India	318	12	2.53	0.52	0.53	2.49	5.32	Yes
OMXC20	Denmark	1740	0	2.59	0.44	1.43	2.52	5.17	No
OMXHPI	Finland	1699	0	2.45	0.50	1.16	2.37	5.47	No
OMXSPI	Sweden	1699	0	2.41	0.51	0.90	2.33	5.09	No
OSEAX	Norway	707	0	2.59	0.48	1.41	2.53	5.41	No
RUT	USA	260	0	2.35	0.51	-3.32	2.30	4.53	Yes
SMSI	Switzerland	1565	0	2.62	0.48	0.38	2.61	4.82	No
SPX	USA	259	0	2.43	0.57	0.56	2.39	4.94	Yes
SSEC	China	467	0	2.67	0.53	1.09	2.61	4.64	Yes
SSMI	Switzerland	259	0	2.40	0.45	1.36	2.31	4.77	Yes
STI	Singapore	2203	1	2.33	0.34	1.39	2.30	4.22	No
S5E	Europe	173	1	2.68	0.53	-1.88	2.66	5.11	Yes

B Dataset

Table 7 and Figure 9 provide a description of the dataset, see the captions for details.

C Empirics of marginal components

The Figures 10, 11, and 12 provide additional results to the analysis presented in Section 5, focusing on the univariate marginal components. They display the same results shown in Figures 4, 5, and 6, but in terms of the autocovariances of each component. The key takeaway is consistent with the one derived from the cross-covariances.

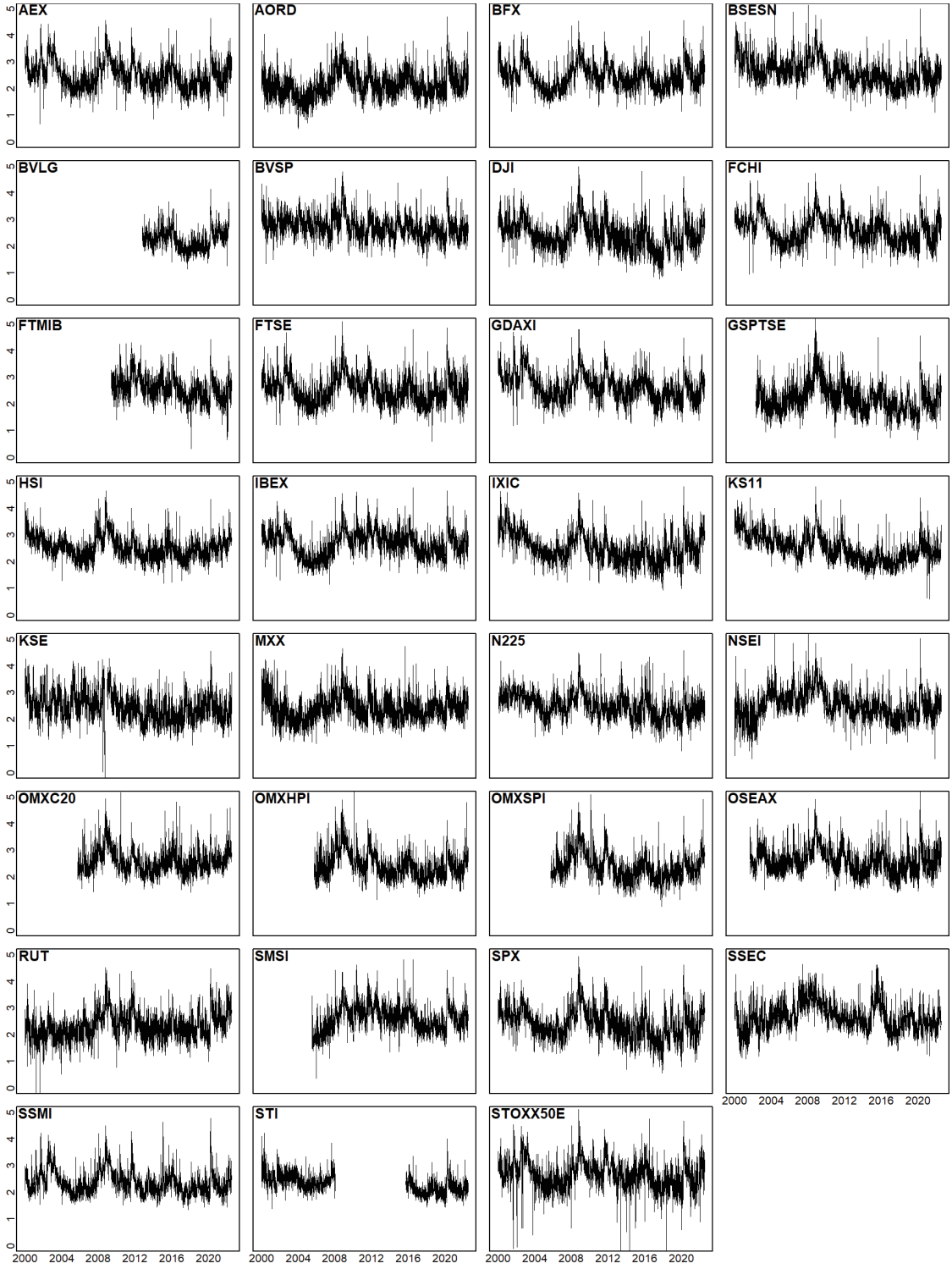

Figure 9: Time series of $\log\left(100\sqrt{RV \times 252}\right)$ for the entire sample, where RV is the realized variance from 5-minute price increments provided in the Oxford-Man realized library. Notice how the symbols not included in the empirical analysis (see Table 7) display prolonged periods of missing values.

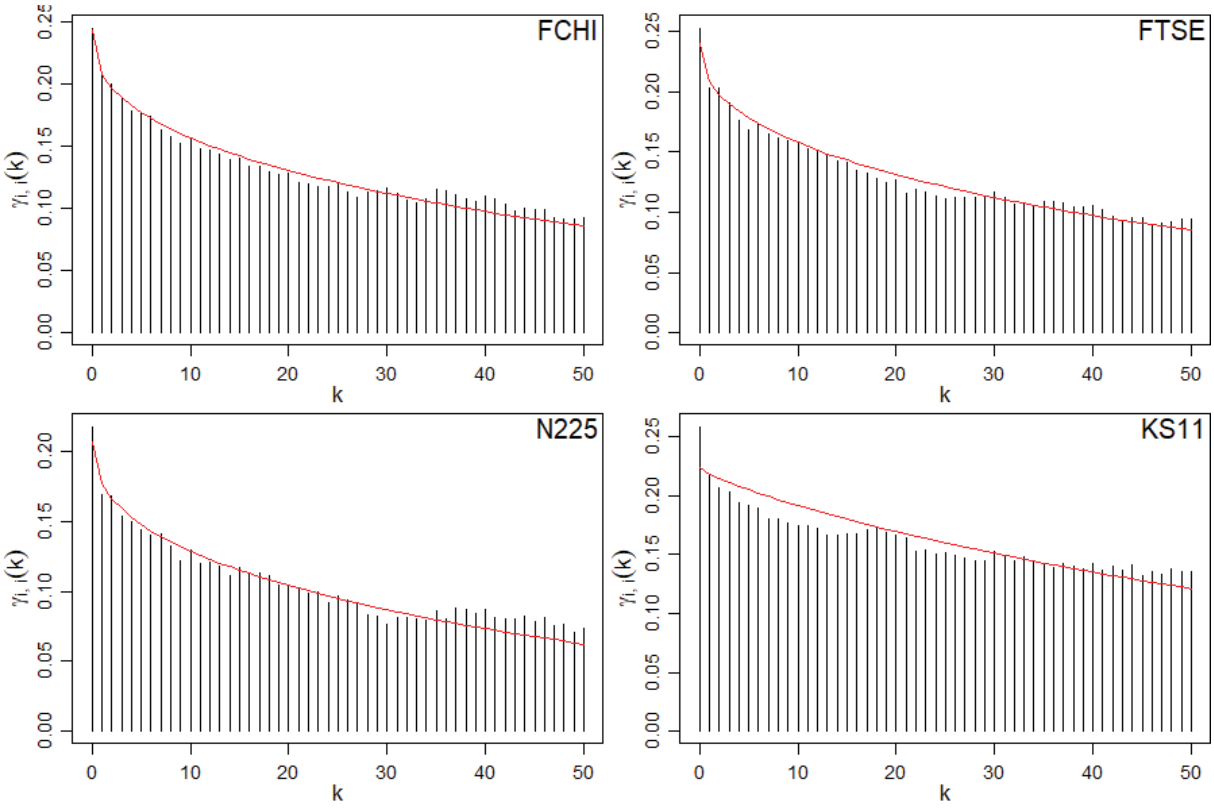

Figure 10: Empirical autocovariances of log-volatilities as bars, alongside the theoretical autocovariances from our model, indicated by the red curves and based on the estimated parameters from Table 3. The panels, arranged from left to right and top to bottom, correspond to the indices FCHI, FTSE, N225, and KS11.

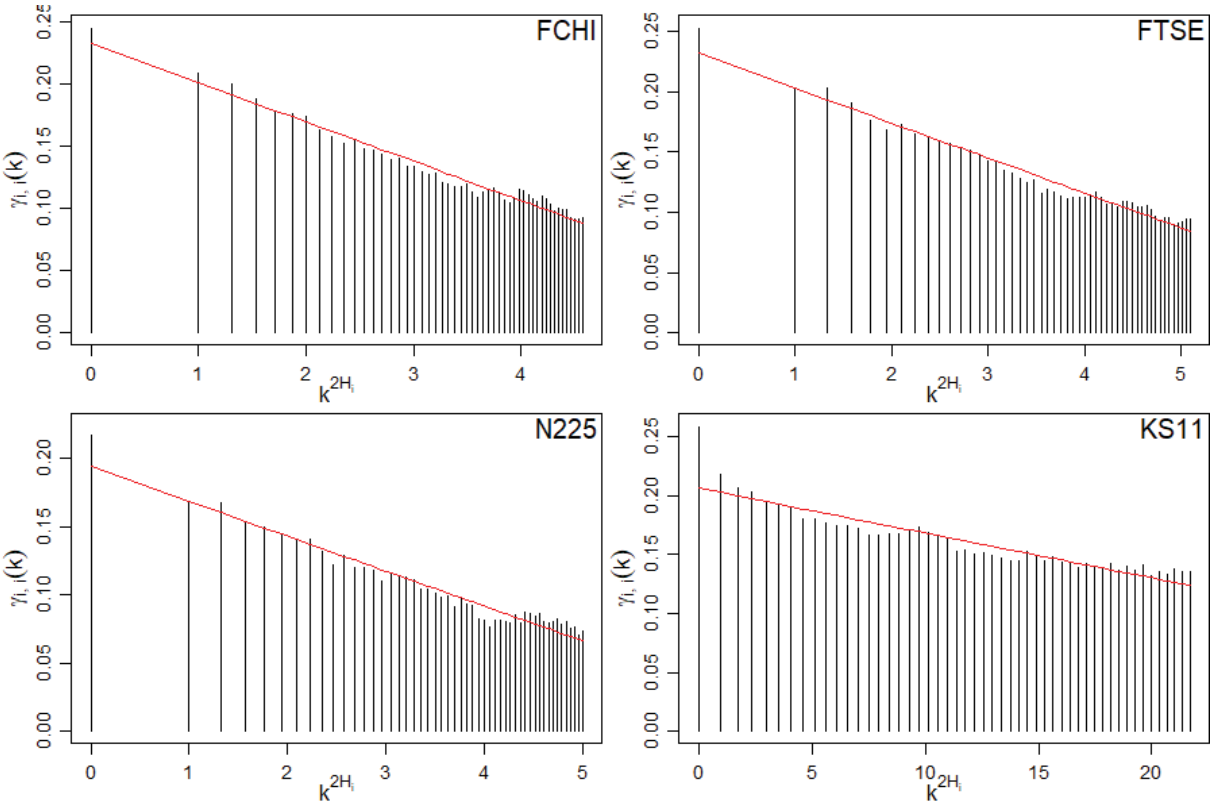

Figure 11: Empirical autocovariances of log-volatilities plotted against a suitable power of the lag (given by twice the Hurst exponent) as bars, alongside the best linear fits, indicated by the red lines. The panels, arranged from left to right and top to bottom, correspond to the indices FCHI, FTSE, N225, and KS11.

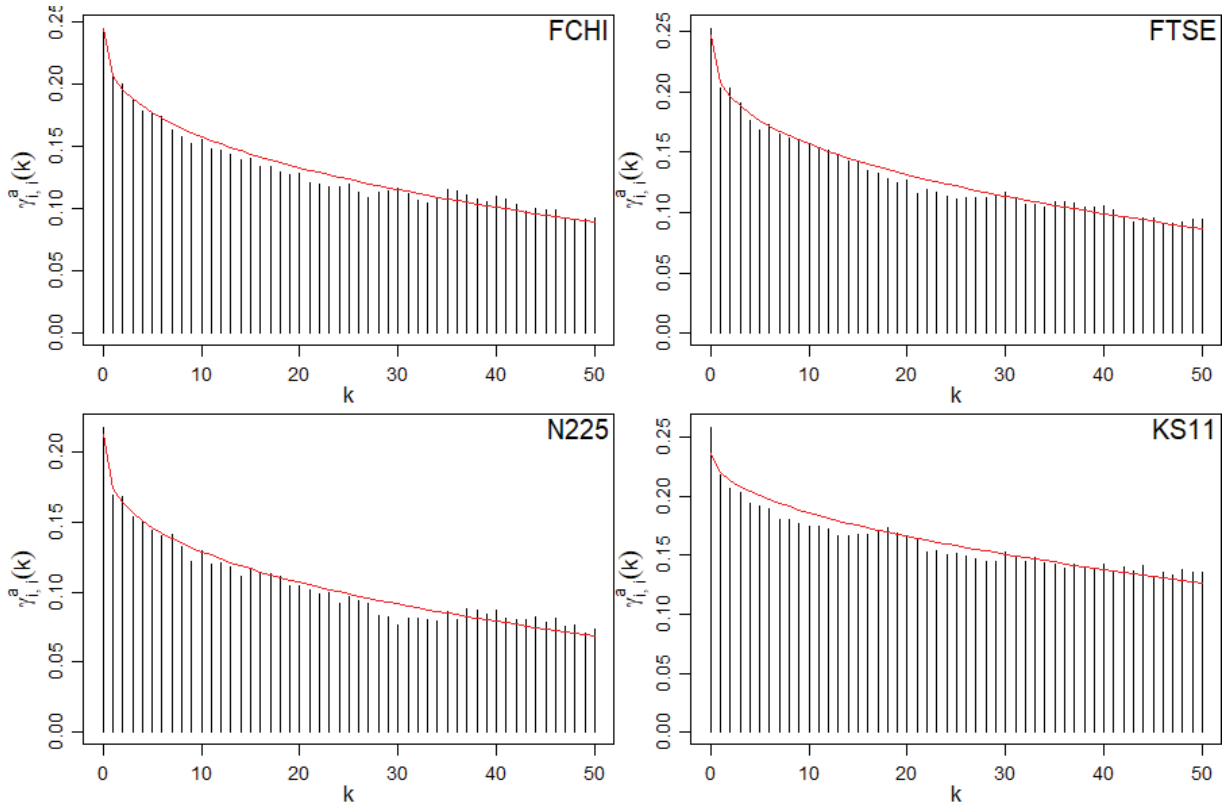

Figure 12: Empirical autocovariances of log-volatilities as bars, alongside the theoretical autocovariances from our model when $\alpha_i \to 0$, indicated by the red curves and based on the estimated parameters (available in the Online Appendix). The panels, arranged from left to right and top to bottom, correspond to the indices FCHI, FTSE, N225, and KS11.

D Spillovers methodology

Starting from a discrete-time moving average representation of a discrete time process $Y_t \in \mathbb{R}^N$,

$$Y_t = \sum_{k=0}^{\infty} A_i \varepsilon_{t-k}, \tag{12}$$

where $\varepsilon_t \overset{iid}{\sim} N(0, \Sigma)$ and $A_i \in \mathbb{R}^{N\times N}$ such that the representation (12) is well-defined, Pesaran (1997) and Pesaran and Shin (1998) show that

$$\begin{aligned}\psi_{i,j}(h) =& \frac{\mathbb{E}\left[\left(Y^i_{t+h} - \mathbb{E}\left[Y^i_{t+h}|\mathcal{F}_{t-1}\right]\right)^2\right] - \mathbb{E}\left[\left(Y^i_{t+h} - \mathbb{E}\left[Y^i_{t+h}|\mathcal{F}_{t-1}, \left(\varepsilon^j_{t+i}\right)_{i=0}^{h}\right]\right)^2\right]}{\mathbb{E}\left[\left(Y^i_{t+h} - \mathbb{E}\left[Y^i_{t+h}|\mathcal{F}_{t-1}\right]\right)^2\right]} \\ =& \frac{\sqrt{\Sigma_{i,i}}^{-1}\sum_{l=0}^{h}\left(e_i^T A_l \Sigma e_j\right)^2}{\sum_{l=0}^{n} e_i^T A_i \Sigma A_i^T e_i},\end{aligned} \tag{13}$$

where $\mathcal{F}_{t-1}$ contains information regarding all the past innovations $\varepsilon_{t-i},\ i = 1, 2, \ldots$. The definition for $\psi_{i,j}(h)$ is used in Diebold and Yilmaz (2012) to construct spillover indices and analyse them. Therefore, we frame the mfOU process in the same setting as above in order to conduct a similar analysis. Consider the representation of the causal mfOU (Dugo et al. 2024):

$$Y_t = \int_{-\infty}^{t} K(t,s) M dW_s, \tag{14}$$

where the kernel $K(t,s) : \mathbb{R}^2 \to \mathbb{R}^N$ is diagonal with components

$$K_i(t,s) = \nu_i \left((t-s)_+^{H_i - \frac{1}{2}} - (-s)_+^{H_i - \frac{1}{2}} - \alpha_i \int_s^t e^{-\alpha_i (t-u)} \left((u-s)_+^{H_i - \frac{1}{2}} - (-s)_+^{H_i - \frac{1}{2}} \right) du \right),$$

$i = 1, \ldots, N$, M is an $N \times N$ matrix such that $MM^T = P$ (from Amblard et al. 2010), with

$$P_{i,j} = \frac{\sin\left(\pi(H_i + H_j)\right)}{B\left(H_i + \frac{1}{2}, H_j + \frac{1}{2}\right)\left(\cos\left(\pi H_i\right) + \cos\left(\pi H_j\right)\right)} \rho_{i,j},$$

where $B(x,y),\ x, y > 0$, denotes the Beta function, and W_t is a standard N-dimensional Brownian motion. Note that the representation in (14) introduces a modification compared to that in Dugo et al. (2024), as it factors M out of the kernel. This factorization enables the separation of the dependence on time from that between components, aligning the model with the framework in (12). Equivalently,

$$\begin{aligned} Y^i_t =& \int_{-\infty}^{t} K_i(t,s) \sum_{j=1}^{N} M_{i,j} dW^j_s \\ =& \sqrt{\frac{\sin(\pi H_i)}{B\left(H_i + \frac{1}{2}, H_i + \frac{1}{2}\right)}} \int_{-\infty}^{t} K_i(t,s) \sum_{j=1}^{N} \sqrt{\frac{B\left(H_i + \frac{1}{2}, H_i + \frac{1}{2}\right)}{\sin(\pi H_i)}} M_{i,j} dW^j_s \\ =& \sqrt{\frac{\sin(\pi H_i)}{B\left(H_i + \frac{1}{2}, H_i + \frac{1}{2}\right)}} \int_{-\infty}^{t} K_i(t,s) \sum_{j=1}^{N} d\overline{W}^j_s \end{aligned}$$

where $\overline{W}$ is a Brownian motion with covariance matrix G, where

$$G_{i,j} = \sqrt{\frac{B(H_i + \frac{1}{2}, H_i + \frac{1}{2}) B(H_j + \frac{1}{2}, H_j + \frac{1}{2})}{\sin\left(\pi H_i\right)\sin\left(\pi H_j\right)}} \frac{1}{B(H_i + \frac{1}{2}, H_j + \frac{1}{2})} \frac{\sin\left(\pi(H_i + H_j)\right)}{\left(\cos\left(\pi H_i\right) + \cos\left(\pi H_j\right)\right)} \rho_{i,j}.$$

Note that $\overline{W}^j_\cdot$ is a Brownian motion with unit variance, for any j. We can rewrite

$$Y_t = \int_0^t \overline{K}(t-s)d\overline{W}_s + \int_{-\infty}^0 K^*(t,s)d\overline{W}_s,$$

where $K^*(t,s) = K(t,s)\sqrt{\sin(\pi H_i)/B(H_i+1/2, H_i+1/2)}$ and

$$\overline{K}(t-s)_{i,j} = \nu_i \sqrt{\frac{\sin(\pi H_i)}{B\left(H_i+\frac{1}{2}, H_i+\frac{1}{2}\right)}} \left((t-s)^{H_i-\frac{1}{2}} - \alpha_i \int_s^t e^{-\alpha_i(t-u)} \left((u-s)^{H_i-\frac{1}{2}} \right) du \right).$$

One can check that this dependens only on $t-s$ with simple change of variables. At this point we can approximate the process using a left point discretization scheme over a grid with uniform mesh Δ, introducing $\varepsilon_l := \Delta_l \overline{W} = \overline{W}_{l\Delta} - \overline{W}_{(l-1)\Delta}$, as

$$\begin{aligned} Y_t &\approx \sum_{l=1}^{\frac{t}{\Delta}} \overline{K}\left(t-(l-1)\Delta\right)\Delta_l\overline{W} + \sum_{l=-\infty}^{0} K^*\left(t,(l-1)\Delta\right)\Delta_l\overline{W} \\ &= \sum_{k=0}^{\frac{t}{\Delta}-1} \overline{K}\left((k+1)\Delta\right)\varepsilon_{\frac{t}{\Delta}-k} + \sum_{k=\frac{t}{\Delta}}^{+\infty} K^*(t,t-(k+1)\Delta)\varepsilon_{\frac{t}{\Delta}-k} \\ &= \sum_{k=0}^{t-1} A_k\varepsilon_{t-k} + \sum_{k=t}^{\infty} B_{k,t}\varepsilon_{t-k}, \end{aligned} \tag{15}$$

where we fix $t := \frac{t}{\Delta}$, $k+l=t$, $A_k = \overline{K}\left((k+1)\Delta\right)$, and $B_{k,t} = K^*\left(t,t-(k+1)\Delta\right)$. When $t \geq h > 0$, the calculation in (13) delivers the same result for the discretized mfOU process in (15) as for the process in (12), due to the common convolution term $\sum_{k=0}^{t-1} A_k\varepsilon_{t-k}$, and therefore

$$\begin{aligned} \psi_{i,j}(h) =& \frac{\Delta\sqrt{\Sigma_{j,j}}^{-1}\sum_{l=0}^{h-1}\left(e_i^T\overline{K}\left((l+1)\Delta\right)Ge_j\right)^2}{\sum_{l=0}^{h-1}\left(e_i^T\overline{K}\left((l+1)\Delta\right)G\overline{K}\left((l+1)\Delta\right)^T e_i\right)} \\ =& \frac{\Delta\sum_{l=0}^{h-1}\overline{K}_{i,j}^2\left((l+1)\Delta\right)G_{i,j}^2}{\sqrt{\Sigma_{j,j}}\sum_{l=0}^{h-1}\overline{K}_{i,j}^2\left((l+1)\Delta\right)G_{i,i}} \\ =& \frac{\Delta G_{i,j}^2}{\sqrt{G_{j,j}}G_{i,i}}, \end{aligned} \tag{16}$$

and

$$\widetilde{\psi}_{i,j} = \frac{\psi_{i,j}}{\sum_{j=1}^N \psi_{i,j}} = \frac{G_{i,j}^2/\sqrt{G_{j,j}}}{\sum_{m=1}^N G_{i,m}^2/\sqrt{G_{m,m}}}. \tag{17}$$

Remark 3. *The result in (17) is obtained under the assumption that ε^j_{t+i}, $i=0,\ldots,n$, $j=1,\ldots,N$ follows a white noise process in (12). A similar spillover analysis could be performed by relaxing the i.i.d. assumption and, instead of using the moving average representation, simply conditioning on ε^j_{t+i}, $i=1,\ldots,n$, $j=1,\ldots,N$ being the fractional Gaussian noise innovations in (13). Preliminary results on this variant suggest qualitatively similar outcomes, though with dependency on the forecast horizon and larger computational burden.*

E Additional material

The Online Appendix, available at https://ranieridugo.github.io/mfou, provides additional empirical results for the components of the system not reported here, as well as results related to the small-alpha (slow mean reversion) and causal regimes. The working code to reproduce the empirical findings of this paper and efficiently simulate a bivariate version of the mfOU process is accessible at the same GitHub repository.

References

Amblard, Pierre-Olivier and Jean-François Coeurjolly (2011). "Identification of the multivariate fractional Brownian motion". In: *IEEE Transactions on Signal Processing* 59.11, pp. 5152–5168.

Amblard, Pierre-Olivier, Jean-François Coeurjolly, Frédéric Lavancier, and Anne Philippe (2010). "Basic properties of the multivariate fractional Brownian motion". In: *arXiv preprint arXiv:1007.0828*.

Andersen, Torben G, Tim Bollerslev, Francis X Diebold, and Heiko Ebens (2001). "The distribution of realized stock return volatility". In: *Journal of financial economics* 61.1, pp. 43–76.

Andersen, Torben G and Bent E Sørensen (1996). "GMM estimation of a stochastic volatility model: A Monte Carlo study". In: *Journal of Business & Economic Statistics* 14.3, pp. 328–352.

Arcones, Miguel A (1994). "Limit theorems for nonlinear functionals of a stationary Gaussian sequence of vectors". In: *The Annals of Probability*, pp. 2242–2274.

Bayer, Christian, Peter K. Friz, and Jim Gatheral (2016). "Pricing under rough volatility". In: *Quantitative Finance* 16.6, pp. 887–904.

Bayer, Christian, Peter K. Friz, A. Gulisashvili, B. Horvath, and B. Stemper (2019). "Short-time near-the-money skew in rough fractional volatility models". In: *Quant. Finance* 19.5, pp. 779–798.

Bennedsen, Mikkel, Asger Lunde, and Mikko S. Pakkanen (2021). "Decoupling the Short- and Long-Term Behavior of Stochastic Volatility". In: *Journal of Financial Econometrics* 20.5, pp. 961–1006.

Bianchi, Sergio, Daniele Angelini, Augusto Pianese, and Massimiliano Frezza (2023). "Rough volatility via the Lamperti transform". In: *Communications in Nonlinear Science and Numerical Simulation* 127, p. 107582.

Bolko, Anine E, Kim Christensen, Mikko S Pakkanen, and Bezirgen Veliyev (2023). "A GMM approach to estimate the roughness of stochastic volatility". In: *Journal of Econometrics* 235.2, pp. 745–778.

Cheridito, Patrick, Hideyuki Kawaguchi, and Makoto Maejima (2003). "Fractional ornstein-uhlenbeck processes". In: *Electronic Journal of probability* 8, pp. 1–14.

Chong, Carsten H., Marc Hoffmann, Yanghui Liu, Mathieu Rosenbaum, and Grégoire Szymanski (June 2024a). "Statistical inference for rough volatility: Central limit theorems". In: *The Annals of Applied Probability* 34.3.

Chong, Carsten H., Marc Hoffmann, Yanghui Liu, Mathieu Rosenbaum, and Grégoire Szymansky (2024b). "Statistical inference for rough volatility: Minimax theory". In: *The Annals of Statistics* 52.4, pp. 1277 –1306.

Comte, Fabienne and Eric Renault (1998). "Long memory in continuous-time stochastic volatility models". In: *Math. Finance* 8.4, pp. 291–323.

Cordi, Marcus, Damien Challet, and Serge Kassibrakis (2021). "The market nanostructure origin of asset price time reversal asymmetry". In: *Quantitative Finance* 21.2, pp. 295–304.

Delemotte, Jules, Stefano De Marco, and Florent Segonne (2023). "Tests for Hurst effect". In: *Available at SSRN: https://ssrn.com/abstract=4428407*.

Diebold, Francis X and Kamil Yilmaz (2009). "Measuring financial asset return and volatility spillovers, with application to global equity markets". In: *The Economic Journal* 119.534, pp. 158–171.

Diebold, Francis X and Kamil Yilmaz (2012). "Better to give than to receive: Predictive directional measurement of volatility spillovers". In: *International Journal of forecasting* 28.1, pp. 57–66.

Ding, Zhuanxin and Clive WJ Granger (1996). "Modeling volatility persistence of speculative returns: a new approach". In: *Journal of econometrics* 73.1, pp. 185–215.

Dugo, Ranieri, Giacomo Giorgio, and Paolo Pigato (2024). "The multivariate fractional Ornstein-Uhlenbeck process". In: *arXiv preprint arXiv:2408.03051*.

Eumenius-Schulz, Yaroslav (2020). "Spot estimation for fractional Ornstein-Uhlenbeck stochastic volatility model: consistency and central limit theorem". In: *Stat. Inference Stoch. Process.* 23.2, pp. 355–380.

Fouque, Jean-Pierre, George Papanicolaou, and K Ronnie Sircar (2000). "Mean-reverting stochastic volatility". In: *International Journal of theoretical and applied finance* 3.01, pp. 101–142.

Friz, Peter K., Paul Gassiat, and Paolo Pigato (2022). "Short-dated smile under rough volatility: asymptotics and numerics". In: *Quantitative Finance* 22.3, pp. 463–480.

Fukasawa, Masaaki, Tetsuya Takabatake, and Rebecca Westphal (2022). "Consistent estimation for fractional stochastic volatility model under high-frequency asymptotics". In: *Mathematical Finance* 32.4, pp. 1086–1132.

Gatheral, Jim, Thibault Jaisson, and Mathieu Rosenbaum (2018). "Volatility is rough". In: *Quantitative Finance* 18.6, pp. 933–949.

Guyon, Julien and Mehdi El Amrani (2023). "Does the Term-Structure of the At-the-Money Skew Really Follow a Power Law?" In: *Risk*.

Hansen, Lars Peter (1982). "Large sample properties of generalized method of moments estimators". In: *Econometrica: Journal of the econometric society*, pp. 1029–1054.

Hayashi, Fumio (2011). *Econometrics*. Princeton University Press.

Jacod, Jean (2000). "Non-parametric Kernel Estimation of the Coefficient of a Diffusion". In: *Scandinavian Journal of Statistics* 27.1, pp. 83–96.

Lang, Gabriel and François Roueff (2001). "Semi-parametric estimation of the Hölder exponent of a stationary Gaussian process with minimax rates". In: *Statistical Inference for Stochastic Processes* 4, pp. 283–306.

Livieri, Giulia, Saad Mouti, Andrea Pallavicini, and Mathieu Rosenbaum (2018). "Rough volatility: Evidence from option prices". In: *IISE Transactions* 50.9, pp. 767–776.

Pesaran, Hashem (1997). *Working with Microfit 4.0: Interactive Econometric Analysis*.

Pesaran, Hashem and Yongcheol Shin (1998). "Generalized impulse response analysis in linear multivariate models". In: *Economics letters* 58.1, pp. 17–29.

Podobnik, Boris, D. Fu, H. Stanley, and Plamen Ivanov (2008). "Detrended cross-correlation analysis: a new method for analyzing two nonstationary time series". In: *Phys Rev Lett*.

Podobnik, Boris, DF Fu, H Eugene Stanley, and P Ch Ivanov (2007). "Power-law autocorrelated stochastic processes with long-range cross-correlations". In: *The European Physical Journal B* 56.1, pp. 47–52.

Podobnik, Boris, Duan Wang, Davor Horvatic, Ivo Grosse, and H Eugene Stanley (2010). "Time-lag cross-correlations in collective phenomena". In: *EPL (Europhysics Letters)* 90.6, p. 68001.

Tieslau, Margie A., Peter Schmidt, and Richard T. Baillie (1996). "A minimum distance estimator for long-memory processes". In: *Journal of Econometrics* 71.1, pp. 249–264.

Wang, Duan, Boris Podobnik, Davor Horvatic, and H. Eugene Stanley (2011). "Quantifying and modeling long-range cross correlations in multiple time series with applications to world stock indices". In: *Phys. Rev. E* 83 (4), p. 046121.

Wang, Xiaohu, Weilin Xiao, and Jun Yu (2023). "Modeling and forecasting realized volatility with the fractional Ornstein-Uhlenbeck process". In: *J. Econometrics* 232.2, pp. 389–415.

Wood, Andrew TA and Grace Chan (1994). "Simulation of stationary Gaussian processes in [0, 1] d". In: *Journal of computational and graphical statistics* 3.4, pp. 409–432.

Zumbach, Gilles (2009). "Time reversal invariance in finance". In: *Quantitative Finance* 9.5, pp. 505–515.

RECENT PUBLICATIONS BY *CEIS Tor Vergata*

With a Little Help from Nurseries. Childcare Services and Mothers' Employment in Italy
Chiara Puccioni and Daniela Vuri
CEIS *Research Paper*, 588 December 2024

SMEs Performance in Public Procurement and the Italian Legality Rating
Andrea Fazio, Erminia Florio and Gustavo Piga
CEIS *Research Paper*, 587 December 2024

A Reinforcement Learning Algorithm For Option Hedging
Federico Giorgi, Stefano Herzel and Paolo Pigato
CEIS *Research Paper*, 586 December 2024

The Long-Run Effects of R&D Subsidies on High-Tech Start-Ups: Insights From Italy
Christoph Koenig, Letizia Borgomeo and Martina Miotto
CEIS *Research Paper*, 585 October 2024

With a Little Help From the Crowd: Estimating Election Fraud with Forensic Methods
Christoph Koenig
CEIS *Research Paper*, 584 October 2024

Biases and Nudges in the Circular Economy: A Review
Luca Congiu, Enrico Botta and Mariangela Zoli
CEIS *Research Paper*, 583 October 2024

Energy Shocks, Pandemics and the Macroeconomy
Luisa Corrado, Stefano Grassi, Aldo Paolillo and Francesco Ravazzolo
CEIS *Research Paper*, 582 August 2024

The Multivariate Fractional Ornstein-Uhlenbeck Process
Ranieri Dugo, Giacomo Giorgio and Paolo Pigato
CEIS *Research Paper*, 581 August 2024

The Macro Neutrality of Exchange-Rate Regimes in the presence of Exporter-Importer Firms
Cosimo Petracchi
CEIS *Research Paper*, 580 July 2024

Monetary Regimes and Real Exchange Rates: Long-Run Evidence at the Product Level
Jason Kim, Marco Mello and Cosimo Petracchi
CEIS *Research Paper*, 579 June 2024

DISTRIBUTION

Our publications are available online at www.ceistorvergata.it

DISCLAIMER

The opinions expressed in these publications are the authors' alone and therefore do not necessarily reflect the opinions of the supporters, staff, or boards of CEIS Tor Vergata.

COPYRIGHT

MEDIA INQUIRIES AND INFORMATION

For media inquiries, please contact Barbara Piazzi at +39 06 72595652/01 or by e-mail at piazzi@ceis.uniroma2.it. Our web site, www.ceistorvergata.it, contains more information about Center's events, publications, and staff.

DEVELOPMENT AND SUPPORT

For information about contributing to CEIS Tor Vergata, please contact at +39 06 72595601 or by e-mail at segr.ceis@economia.uniroma2.it